

This figure "Dusit\_Niyato.jpg" is available in "jpg" format from:

<http://arxiv.org/ps/2002.12271v4>

This figure "Helin\_Yang.jpg" is available in "jpg" format from:

<http://arxiv.org/ps/2002.12271v4>

# Deep Reinforcement Learning Based Intelligent Reflecting Surface for Secure Wireless Communications

Helin Yang, *Student Member, IEEE*, Zehui Xiong, *Student Member, IEEE*, Jun Zhao, *Member, IEEE*, Dusit Niyato, *Fellow, IEEE*, Liang Xiao, *Senior Member, IEEE*, and Qingqing Wu, *Member, IEEE*

**Abstract**—In this paper, we study an intelligent reflecting surface (IRS)-aided wireless secure communication system, where an IRS is deployed to adjust its reflecting elements to secure the communication of multiple legitimate users in the presence of multiple eavesdroppers. Aiming to improve the system secrecy rate, a design problem for jointly optimizing the base station (BS)'s beamforming and the IRS's reflecting beamforming is formulated considering different quality of service (QoS) requirements and time-varying channel conditions. As the system is highly dynamic and complex, and it is challenging to address the non-convex optimization problem, a novel deep reinforcement learning (DRL)-based secure beamforming approach is firstly proposed to achieve the optimal beamforming policy against eavesdroppers in dynamic environments. Furthermore, post-decision state (PDS) and prioritized experience replay (PER) schemes are utilized to enhance the learning efficiency and secrecy performance. Specifically, a modified PDS scheme is presented to trace the channel dynamic and adjust the beamforming policy against channel uncertainty accordingly. Simulation results demonstrate that the proposed deep PDS-PER learning based secure beamforming approach can significantly improve the system secrecy rate and QoS satisfaction probability in IRS-aided secure communication systems.

This research is supported by the National Research Foundation (NRF), Singapore, under Singapore Energy Market Authority (EMA), Energy Resilience, NRF2017EWT-EP003-041, Singapore NRF2015-NRF-ISF001-2277, Singapore NRF National Satellite of Excellence, Design Science and Technology for Secure Critical Infrastructure NSoE DeST-SCI2019-0007, A\*STAR-NTU-SUTD Joint Research Grant on Artificial Intelligence for the Future of Manufacturing RGANS1906, Wallenberg AI, Autonomous Systems and Software Program and Nanyang Technological University (WASP/NTU) under grant M4082187 (4080), Singapore Ministry of Education (MOE) Tier 1 (RG16/20), and NTU-WeBank JRI (NWJ-2020-004), Alibaba Group through Alibaba Innovative Research (AIR) Program, Alibaba-NTU Singapore Joint Research Institute (JRI), Nanyang Technological University (NTU) Startup Grant, Singapore Ministry of Education Academic Research Fund Tier 1 RG128/18, Tier 1 RG115/19, Tier 1 RT07/19, Tier 1 RT01/19, and Tier 2 MOE2019-T2-1-176, NTU-WASP Joint Project, Singapore National Research Foundation under its Strategic Capability Research Centres Funding Initiative: Strategic Centre for Research in Privacy-Preserving Technologies & Systems, Energy Research Institute @NTU, Singapore NRF National Satellite of Excellence, Design Science and Technology for Secure Critical Infrastructure NSoE DeST-SCI2019-0012, AI Singapore 100 Experiments (100E) programme, NTU Project for Large Vertical Take-Off & Landing Research Platform, and the Natural Science Foundation of China under Grant 61971366. A part of this paper was accepted in IEEE Global Communications Conference, December 2020, Taipei, Taiwan [40]. (*Corresponding author: Zehui Xiong.*)

H. Yang, Z. Xiong, J. Zhao, and D. Niyato are with the School of Computer Science and Engineering, Nanyang Technological University, Singapore 639798 (e-mail: hyang013@e.ntu.edu.sg, zxiong002@e.ntu.edu.sg, junzhao@ntu.edu.sg, dniyato@ntu.edu.sg).

L. Xiao is with the Department of Information and Communication Engineering, Xiamen University, Xiamen 361005, China (e-mail: lxiao@xmu.edu.cn).

Q. Wu is with State Key Laboratory of Internet of Things for Smart City, University of Macau, Macau, 999078 China. (email:qingqingwu@um.edu.mo).

**Index Terms**—Secure communication, intelligent reflecting surface, beamforming, secrecy rate, deep reinforcement learning.

## I. INTRODUCTION

PHYSICAL layer security (PLS) has attracted increasing attention as an alternative of cryptography-based techniques for wireless communications [1], where PLS exploits the wireless channel characteristics by using signal processing designs and channel coding to support secure communication services without relying on a shared secret key [1], [2]. So far, a variety of approaches have been reported to improve PLS in wireless communication systems, e.g., cooperative relaying strategies [3], [4], artificial noise-assisted beamforming [5], [6], and cooperative jamming [7], [8]. However, employing a large number of active antennas and relays in PLS systems incurs an excessive hardware cost and the system complexity. Moreover, cooperative jamming and transmitting artificial noise require extra transmit power for security guarantees.

To tackle these shortcomings of the existing approaches [3]-[8], a new paradigm, called intelligent reflecting surface (IRS) [9]-[13], has been proposed as a promising technique to achieve high spectrum efficiency and energy efficiency, and enhance secrecy rate in the fifth generation (5G) and beyond wireless communication systems. In particular, IRS is a uniform planar array which is comprised of a number of low-cost passive reflecting elements, where each of elements adaptively adjusts its reflection amplitude and/or phase to control the strength and direction of the electromagnetic wave, hence IRS is capable of enhancing and/or weakening the reflected signals at different users [9]. As a result, the reflected signal by IRS can increase the received signal at legitimate users while suppressing the signal at the eavesdroppers [9]-[13]. Hence, from the PLS perspective, some innovative studies have been recently devoted to performance optimization for IRS-aided secure communications [14]-[25].

### A. Related Works

Initial studies on IRS-aided secure communication systems have reported in [14]-[17], where a simple system model with only a single-antenna legitimate user and a single-antenna eavesdropper was considered in these works. The authors in [14] and [15] applied the alternative optimization (AO) algorithm to jointly optimize the transmit beamforming vector at the base station (BS) and the phase elements at the IRS for the maximization of the secrecy rate, but they did not extend their models to multi-user IRS-assisted secure

communication systems. To minimize the transmit power at the BS subject to the secrecy rate constraint, the authors in [18] utilized AO solution and semidefinite programming (SDP) relaxation to address the optimization problem with the objective to jointly optimize the power allocation and the IRS reflecting beamforming. In addition, Feng *et al.* [19] also studied the secure transmission framework with an IRS to minimize the system transmit power in cases of rank-one and full-rank BS-IRS links, and derived a closed-form expression of beamforming matrix. Different from these studies [14]-[19] which considered only a single eavesdropper, secure communication systems comprising multiple eavesdroppers were investigated in [20]-[22]. Chen *et al.* [20] presented a minimum-secrecy-rate maximization design to provide secure communication services for multiple legitimate users while keeping them secret from multiple eavesdroppers in an IRS-aided multi-user multiple-input single-output (MISO) system, but the simplification of the optimization problem may cause a performance loss. The authors in [23] and [24] studied an IRS-aided multiple-input multiple-output (MIMO) channel, where a multi-antenna BS transmits data stream to a multi-antenna legitimate user in the presence of an eavesdropper configured with multiple antennas, and a suboptimal secrecy rate maximization approach was presented to optimize the beamforming policy. In addition to the use of AO or SDP in the system performance optimization, the minorization-maximization (MM) algorithm was recently utilized to optimize the joint transmit beamforming at the BS and phase shift coefficient at the IRS [16], [23].

Moreover, the authors in [22] and [25] employed the artificial noise-aided beamforming for IRS-aided MISO secure communication systems to improve the system secrecy rate, and an AO based solution was applied to jointly optimize the BS's beamforming, artificial noise interference vector and IRS's reflecting beamforming with the goal to maximize the secrecy rate. All these existing studies [14]-[20], [22]-[25] assumed that perfect channel state information (CSI) of legitimate users or eavesdroppers is available at the BS, which is not a practical assumption. The reason is that acquiring perfect CSI at the BS is challenging since the corresponding CSI may be outdated when the channel is time-varying due to the transmission delay, processing delay, and high mobility of users. Hence, Yu *et al.* [21] investigated an optimization problem with considering the impacts of outdated CSI of the eavesdropping channels in an IRS-aided secure communication system, and a robust algorithm was proposed to address the optimization problem in the presence of multiple eavesdroppers.

The above mentioned studies [14]-[25] mainly applied the traditional optimization techniques e.g., AO, SDP or MM algorithms to jointly optimize the BS's beamforming and the IRS's reflecting beamforming in IRS-aided secure communication systems, which are less efficient for large-scale systems. Inspired by the recent advances of artificial intelligence (AI), several works attempted to utilize AI algorithms to optimize IRS's reflecting beamforming [26]-[29]. Deep learning (DL) was exploited to search the optimal IRS reflection matrices that maximize the achievable system rate in an IRS-aided

communication system, and the simulation demonstrated that DL significantly outperforms conventional algorithms. Moreover, the authors in [28] and [29] proposed deep reinforcement learning (DRL) based approach to address the non-convex optimization problem, and the phase shifts at the IRS are optimized effectively. However, the works [26]-[29] merely considered to maximize the system achievable rate of a single user without considering the scenario of multiple users, secure communication and imperfect CSI in their models. The authors in [30] and [31] applied reinforcement learning (RL) to achieve smart beamforming at the BS against an eavesdropper in complex environments, but the IRS-aided secure communication system needs to optimize the IRS's reflect beamforming in addition to the BS's transmit beamforming. To the best of our knowledge, RL or DRL has not been explored yet in prior works to optimize both the BS's transmit beamforming and the IRS's reflect beamforming in dynamic IRS-aided secure communication systems, under the condition of multiple eavesdroppers and imperfect CSI, which thus motivates this work.

## B. Contributions

In this paper, we investigate an IRS-aided secure communication system with the objective to maximize the system secrecy rate of multiple legitimate users in the presence of multiple eavesdroppers under realistic time-varying channels, while guaranteeing quality of service (QoS) requirements of legitimate users. A novel DRL-based secure beamforming approach is firstly proposed to jointly optimize the beamforming matrix at the BS and the reflecting beamforming matrix (reflection phases) at the IRS in dynamic environments. The major contributions of this paper are summarized as follows:

- The physical secure communication based on IRS with multiple eavesdroppers is investigated under the condition of time-varying channel coefficients in this paper. In addition, we formulate a joint BS's transmit beamforming and IRS's reflect beamforming optimization problem with the goal of maximizing the system secrecy rate while considering the QoS requirements of legitimate users.
- An RL-based intelligent beamforming framework is presented to achieve the optimal BS's beamforming and the IRS's reflecting beamforming, where the central controller intelligently optimizes the beamforming policy by using a Markov decision process (MDP) according to the instantaneous observations from dynamic environment. Specifically, a QoS-aware reward function is constructed by covering both the secrecy rate and users' QoS requirements into the learning process.
- A DRL-based secure beamforming approach is proposed to improve the learning efficiency and secrecy performance by fully exploiting the information of complex structure of the beamforming policy domain, where a modified post-decision state (PDS) learning is presented to trace the channel dynamic against channel uncertainty, and prioritized experience replay (PER) is applied to enhance the learning efficiency.
- Extensive simulation results are provided to demonstrate the effectiveness of the proposed deep PDS-PER learning

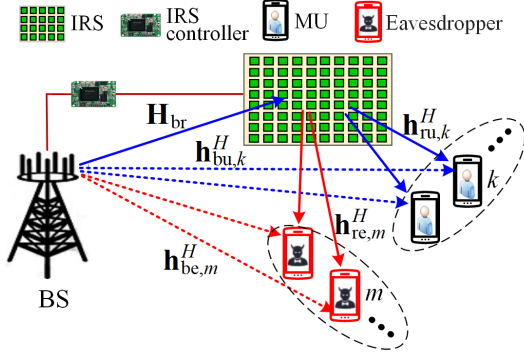


Fig. 1. IRS-aided secure communication under multiple eavesdroppers.

based secure beamforming approach in terms of improving the secrecy rate and the QoS satisfaction probability, compared with other existing approaches. For instance, the proposed learning approach achieves the secrecy rate and QoS satisfaction level improvements of 17.21% and 8.67%, compared with the approach [14] in time-varying channel condition.

The rest of this paper is organized as follows. Section II presents the system model and problem formulation. The optimization problem is formulated as an RL problem in Section III. Section IV proposes a deep PDS-PER based secure beamforming approach. Section V provides simulation results and Section VI concludes the paper.

Notations: In this paper, vectors and matrices are represented by Boldface lowercase and uppercase letters, respectively.  $\text{Tr}(\cdot)$ ,  $(\cdot)^*$  and  $(\cdot)^H$  denote the trace, the conjugate and the conjugate transpose operations, respectively.  $|\cdot|$  and  $\|\cdot\|$  stand for the absolute value of a scalar and the Euclidean norm of a vector or matrix, respectively.  $\mathbb{E}[\cdot]$  denotes the expectation operation.  $\mathbb{C}^{M \times N}$  represents the space of complex-valued matrices.

## II. SYSTEM MODEL AND PROBLEM FORMULATION

### A. System Model

We consider an IRS-aided secure communication system, as shown in Fig. 1, where the BS is equipped with  $N$  antennas to serve  $K$  single-antenna legitimate mobile users (MUs) in the presence of  $M$  single-antenna eavesdroppers. An IRS with  $L$  reflecting elements is deployed in the system to assist secure wireless communications from the BS to the MUs. The IRS is equipped with a controller to coordinate with the BS. For the ease of practical implementation, the maximal reflection without power loss at the IRS is considered since the reflecting elements are designed to maximize the reflected desired signal power to the MUs [13]-[23]. In addition, unauthorized eavesdroppers aim to eavesdrop any of the data streams of the MUs. Hence, the use of reflecting beamforming at IRS is also investigated to improve the achievable secrecy rate at the MUs while suppressing the wiretapped data rate at the eavesdroppers. In addition, we explicitly state that the eavesdroppers cannot collide [5], [6], [18]-[21].

Let  $\mathcal{K} = \{1, 2, \dots, K\}$ ,  $\mathcal{M} = \{1, 2, \dots, M\}$  and  $\mathcal{L} = \{1, 2, \dots, L\}$  denote the MU set, the eavesdropper set and the IRS reflecting element set, respectively. Let  $\mathbf{H}_{\text{br}} \in \mathbb{C}^{L \times N}$ ,  $\mathbf{h}_{\text{bu},k}^H \in \mathbb{C}^{1 \times N}$ ,  $\mathbf{h}_{\text{ru},k}^H \in \mathbb{C}^{1 \times L}$ ,  $\mathbf{h}_{\text{be},m}^H \in \mathbb{C}^{1 \times N}$ , and  $\mathbf{h}_{\text{re},m}^H \in \mathbb{C}^{1 \times L}$  denote the channel coefficients from the BS to the IRS, from the BS to the  $k$ -th MU, from the IRS to the  $k$ -th MU, from the BS to the  $m$ -th eavesdropper, and from the IRS to the  $m$ -th eavesdropper, respectively. All the above mentioned channel coefficients in the system are assumed to be small-scale fading with path loss which follows the Rayleigh fading model [11]-[14], [21]. Let  $\Psi = \text{diag}(\chi_1 e^{j\theta_1}, \chi_2 e^{j\theta_2}, \dots, \chi_L e^{j\theta_L})$  denote the reflection coefficient matrix associated with effective phase shifts at the IRS, where  $\chi_l \in [0, 1]$  and  $\theta_l \in [0, 2\pi]$  denote the amplitude reflection factor and the phase shift coefficient on the combined transmitted signal, respectively. As each phase shift is desired to be designed to achieve full reflection, we consider that  $\chi_l = 1, \forall l \in \mathcal{L}$  in the sequel of the paper.

At the BS side, the beamforming vector for the  $k$ -th MU is denoted as  $\mathbf{v}_k \in \mathbb{C}^{N \times 1}$ , which is the continuous linear precoding [11]-[16], [23]. Thus, the transmitted signal for all MUs at the BS is written as  $\mathbf{x} = \sum_{k=1}^K \mathbf{v}_k s_k$ , where  $s_k$  is the transmitted symbol for the  $k$ -th MU which can be modelled as independent and identically distributed (i.i.d.) random variables with zero mean and unit variance [11]-[16], [23], and  $s_k \sim \mathcal{CN}(0, 1)$ . The total transmit power at the BS is subject to the maximum power constraint:

$$\mathbb{E}[\|\mathbf{x}\|^2] = \text{Tr}(\mathbf{V}\mathbf{V}^H) \leq P_{\max} \quad (1)$$

where  $\mathbf{V} \triangleq [\mathbf{v}_1, \mathbf{v}_2, \dots, \mathbf{v}_K] \in \mathbb{C}^{M \times K}$ , and  $P_{\max}$  is the maximum transmit power at the BS.

When the BS transmits a secret message to the  $k$ -th MU, the MU will receive the signal from the BS and the reflected signal from the IRS. Accordingly, the received signal at MU  $k$  can be given by

$$y_k = \underbrace{(\mathbf{h}_{\text{ru},k}^H \Psi \mathbf{H}_{\text{br}} + \mathbf{h}_{\text{bu},k}^H) \mathbf{v}_k s_k}_{\text{desired signal}} + \underbrace{\sum_{i \in \mathcal{K}, i \neq k} (\mathbf{h}_{\text{ru},k}^H \Psi \mathbf{H}_{\text{br}} + \mathbf{h}_{\text{bu},k}^H) \mathbf{v}_i s_i + n_k}_{\text{inter-user interference}} \quad (2)$$

where  $n_k$  denotes the additive complex Gaussian noise (AWGN) with the with zero mean and variance  $\delta_k^2$  at the  $k$ -th MU. In (2), we observe that in addition to the received desired signal, each MU also suffers inter-user interference (IUI) in the system. In addition, the received signal at eavesdropper  $m$  is expressed by

$$y_m = (\mathbf{h}_{\text{re},m}^H \Psi \mathbf{H}_{\text{br}} + \mathbf{h}_{\text{be},m}^H) \sum_{k \in \mathcal{K}} \mathbf{v}_k s_k + n_m \quad (3)$$

where  $n_m$  is the AWGN of eavesdropper  $m$  with the variance  $\delta_m^2$ .

In practical systems, it is not easy for the BS and the IRS to obtain perfect CSI [9], [21]. This is due to the fact that both the transmission delay and processing delay exist, as well as the mobility of the users. Therefore, CSI is outdated at the time when the BS and the IRS transmit the data stream to MUs

[21]. Once this outdated CSI is employed for beamforming, it will lead to a negative effect on the demodulation at the MUs, thereby leading to substantial performance loss [21]. Therefore, it is necessary to consider outdated CSI in the IRS-aided secure communication system.

Let  $T_{\text{delay}}$  denote the delay between the outdated CSI and the real-time CSI. In other words, when the BS receives the pilot sequences sent from the MUs at the time slot  $t$ , it will complete the channel estimation process and begin to transmit data stream to the MUs at the time slot  $t + T_{\text{delay}}$ . Hence, the relation between the outdated channel vector  $\mathbf{h}(t)$  and the real-time channel vector  $\mathbf{h}(t + T_{\text{delay}})$  can be expressed by

$$\mathbf{h}(t + T_{\text{delay}}) = \rho \mathbf{h}(t) + \sqrt{1 - \rho^2} \hat{\mathbf{h}}(t + T_{\text{delay}}). \quad (4)$$

In (4),  $\hat{\mathbf{h}}(t + T_{\text{delay}})$  is independent identically distributed with  $\mathbf{h}(t)$  and  $\mathbf{h}(t + T_{\text{delay}})$ , and it is with zero-mean and unit-variance complex Gaussian entries.  $\rho$  is the autocorrelation function (outdated CSI coefficient) of the channel gain  $\mathbf{h}(t)$  and  $0 \leq \rho \leq 1$ , which is given by

$$\rho = J_0(2\pi f_D T_{\text{delay}}) \quad (5)$$

where  $J_0(\cdot)$  is the zeroth-order Bessel function of the first kind,  $f_D$  is the Doppler spread which is generally a function of the velocity ( $v$ ) of the transceivers, the carrier frequency ( $f_c$ ) and the speed of light ( $c$ ), i.e.,  $f_D = vf_c/c$ . Note that  $\rho = 1$  indicates the outdated CSI effect is eliminated, whereas  $\rho = 0$  represents no CSI.

As the outdated CSI introduces the channel uncertainty in practical dynamic systems, the actual channel coefficients can be rewritten as

$$\begin{aligned} \mathbf{h}_{\text{bu},k} &= \tilde{\mathbf{h}}_{\text{bu},k} + \Delta \mathbf{h}_{\text{bu},k}, \quad \forall k \in \mathcal{K}, \\ \mathbf{h}_{\text{ru},k} &= \tilde{\mathbf{h}}_{\text{ru},k} + \Delta \mathbf{h}_{\text{ru},k}, \quad \forall k \in \mathcal{K}, \\ \mathbf{h}_{\text{be},m} &= \tilde{\mathbf{h}}_{\text{be},m} + \Delta \mathbf{h}_{\text{be},m}, \quad \forall m \in \mathcal{M}, \\ \mathbf{h}_{\text{re},m} &= \tilde{\mathbf{h}}_{\text{re},m} + \Delta \mathbf{h}_{\text{re},m}, \quad \forall m \in \mathcal{M}, \end{aligned} \quad (6)$$

where  $\tilde{\mathbf{h}}_{\text{bu},k}$ ,  $\tilde{\mathbf{h}}_{\text{ru},k}$ ,  $\tilde{\mathbf{h}}_{\text{be},m}$  and  $\tilde{\mathbf{h}}_{\text{re},m}$  denote the estimated channel vectors;  $\Delta \mathbf{h}_{\text{bu},k}$ ,  $\Delta \mathbf{h}_{\text{ru},k}$ ,  $\Delta \mathbf{h}_{\text{be},m}$  and  $\Delta \mathbf{h}_{\text{re},m}$  are the corresponding channel error vectors. In the paper, generally, the channel error vectors of each MU and each eavesdropper can be bounded with respect to the Euclidean norm by using norm-bounded error model, i.e.,

$$\begin{aligned} \|\Delta \mathbf{h}_{\text{bu}}\|^2 &\leq (\varsigma_{\text{bu}})^2, \quad \|\Delta \mathbf{h}_{\text{ru}}\|^2 \leq (\varsigma_{\text{ru}})^2, \\ \|\Delta \mathbf{h}_{\text{be}}\|^2 &\leq (\varsigma_{\text{be}})^2, \quad \|\Delta \mathbf{h}_{\text{re}}\|^2 \leq (\varsigma_{\text{re}})^2, \end{aligned} \quad (7)$$

where  $\varsigma_{\text{bu}}$ ,  $\varsigma_{\text{ru}}$ ,  $\varsigma_{\text{be}}$ , and  $\varsigma_{\text{re}}$  refer to the radii of the deterministically bounded error regions.

Under the channel uncertainty model, the achievable rate of the  $k$ -th MU is given by

$$R_k^u = \log_2 \left( 1 + \frac{|\mathbf{h}_{\text{ru},k}^H \Psi \mathbf{H}_{\text{br}} + \mathbf{h}_{\text{bu},k}^H \mathbf{v}_k|^2}{\left| \sum_{i \in \mathcal{K}, i \neq k} (\mathbf{h}_{\text{ru},k}^H \Psi \mathbf{H}_{\text{br}} + \mathbf{h}_{\text{bu},k}^H \mathbf{v}_i)^2 + \delta_k^2 \right|} \right). \quad (8)$$

If the  $m$ -th eavesdropper attempts to eavesdrop the signal of the  $k$ -th MU, its achievable rate can be expressed by

$$R_{m,k}^e = \log_2 \left( 1 + \frac{|\mathbf{h}_{\text{re},m}^H \Psi \mathbf{H}_{\text{br}} + \mathbf{h}_{\text{be},m}^H \mathbf{v}_k|^2}{\left| \sum_{i \in \mathcal{K}, i \neq k} (\mathbf{h}_{\text{re},m}^H \Psi \mathbf{H}_{\text{br}} + \mathbf{h}_{\text{be},m}^H \mathbf{v}_i)^2 + \delta_m^2 \right|} \right). \quad (9)$$

Since each eavesdropper can eavesdrop any of the  $K$  MUs' signal, according to [14]-[25], the achievable individual secrecy rate from the BS to the  $k$ -th MU can be expressed by

$$R_k^{\text{sec}} = \left[ R_k^u - \max_{\forall m} R_{m,k}^e \right]^+ \quad (10)$$

where  $[z]^+ = \max(0, z)$ .

### B. Problem Formulation

Our objective is to jointly optimize the robust BS's transmit beamforming matrix  $\mathbf{V}$  and the robust IRS's reflecting beamforming matrix  $\Psi$  from the system beamforming codebook  $\mathcal{F}$  to maximize the worst-case secrecy rate with the worst-case secrecy rate and data rate constraints, the total BS transmit power constraint and the IRS reflecting unit constraint. As such, the optimization problem is formulated as

$$\begin{aligned} \max_{\mathbf{V}, \Psi} \min_{\{\Delta \mathbf{h}\}} \sum_{k \in \mathcal{K}} R_k^{\text{sec}} \\ \text{s.t. (a): } R_k^{\text{sec}} &\geq R_k^{\text{sec}, \min}, \quad \forall k \in \mathcal{K}, \\ \text{(b): } \min_{\substack{\|\Delta \mathbf{h}_{\text{bu}}\|^2 &\leq (\varsigma_{\text{bu}})^2, \\ \|\Delta \mathbf{h}_{\text{ru}}\|^2 &\leq (\varsigma_{\text{ru}})^2}} (R_k^u) &\geq R_k^{\min}, \quad \forall k \in \mathcal{K}, \\ \text{(c): } \text{Tr}(\mathbf{V} \mathbf{V}^H) &\leq P_{\max}, \\ \text{(d): } |\chi e^{j\theta_l}| &= 1, \quad 0 \leq \theta_l \leq 2\pi, \quad \forall l \in \mathcal{L}, \end{aligned} \quad (11)$$

where  $R_k^{\text{sec}, \min}$  is the target secrecy rate of the  $k$ -th MU, and  $R_k^{\min}$  denotes its target data rate. The constraints in (11a) and (11b) are imposed to satisfy the worst-case secrecy rate and data rate requirements, respectively. The constraint in (11c) is set to satisfy the BS's maximum power constraint. The constraint in (11d) is the constraint of the IRS reflecting elements. Obviously, it is challenging to obtain an optimal solution to the optimization (11), since the objective function in (11) is non-concave with respect to either  $\mathbf{V}$  or  $\Psi$ , and the coupling of the optimization variables ( $\mathbf{V}$  and  $\Psi$ ) and the unit-norm constraints in (11d) are non-convex. In addition, we would consider the robust beamforming design to maximize the worst-case achievable secrecy rate of the system while guaranteeing the worst-case constraints.

### III. PROBLEM TRANSFORMATION BASED ON RL

The optimization problem given in (11) is difficult to address as it is a non-convex problem. In addition, in realistic IRS-aided secure communication systems, the capabilities of MUs, the channel quality, and the service applications will change dynamically. Moreover, the problem in (11) is just a single time slot optimization problem, which may converge to a suboptimal solution and obtain the greedy-search like performance due to the ignorance of the historical system state and the long term benefit. Hence, it is generally infeasible to apply the traditional optimization techniques (AO, SDP, and

MM) to achieve an effective secure beamforming policy in uncertain dynamic environments.

Model-free RL is a dynamic programming tool which can be adopted to solve the decision-making problem by learning the optimal solution in dynamic environments [32]. Hence, we model the secure beamforming optimization problem as an RL problem. In RL, the IRS-aided secure communication system is treated as an environment, the central controller at the BS is regarded as a learning agent. The key elements of RL are defined as follows.

**State space:** Let  $\mathcal{S}$  denote the system state space. The current system state  $s \in \mathcal{S}$  includes the channel information of all users, the secrecy rate, the transmission data rate of the last time slot and the QoS satisfaction level, which is defined as

$$s = \left\{ \left\{ \mathbf{h}_k \right\}_{k \in \mathcal{K}}, \left\{ \mathbf{h}_m \right\}_{m \in \mathcal{M}}, \left\{ R_k^{\text{sec}} \right\}_{k \in \mathcal{K}}, \left\{ R_k \right\}_{k \in \mathcal{K}}, \left\{ \text{QoS}_k \right\}_{k \in \mathcal{K}} \right\}, \quad (12)$$

where  $\mathbf{h}_k$  and  $\mathbf{h}_m$  are the channel coefficients of the  $k$ -th MU and  $m$ -th eavesdropper, respectively.  $\text{QoS}_k$  is the feedback QoS satisfaction level of the  $k$ -th MU, where the QoS satisfaction level consists of both the minimum secrecy rate satisfaction level in (11a) and the minimum data rate satisfaction level in (11b). Other parameters in (12) are already defined in Section II.

**Action space:** Let  $\mathcal{A}$  denote the system action space. According to the observed system state  $s$ , the central controller chooses the beamforming vector  $\{\mathbf{v}_k\}_{k \in \mathcal{K}}$  at the BS and the IRS reflecting beamforming coefficient (phase shift)  $\{\theta_l\}_{l \in \mathcal{L}}$  at the IRS. Hence, the action  $a \in \mathcal{A}$  can be defined by

$$a = \left\{ \left\{ \mathbf{v}_k \right\}_{k \in \mathcal{K}}, \left\{ \theta_l \right\}_{l \in \mathcal{L}} \right\}. \quad (13)$$

**Transition probability:** Let  $\mathcal{T}(s'|s, a)$  represent the transition probability, which is the probability of transitioning to a new state  $s' \in \mathcal{S}$ , given the action  $a$  executed in the state  $s$ .

**Reward function:** In RL, the reward acts as a signal to evaluate how good the secure beamforming policy is when the agent executes an action at a current state. The system performance will be enhanced when the reward function at each learning step correlates with the desired objective. Thus, it is important to design an efficient reward function to improve the MUs' QoS satisfaction levels.

In this paper, the reward function represents the optimization objective, and our objective is to maximize the system secrecy rate of all MUs while guaranteeing their QoS requirements. Thus, the presented QoS-aware reward function is expressed as

$$r = \underbrace{\sum_{k \in \mathcal{K}} R_k^{\text{sec}}}_{\text{part 1}} - \underbrace{\sum_{k \in \mathcal{K}} \mu_1 p_k^{\text{sec}}}_{\text{part 2}} - \underbrace{\sum_{k \in \mathcal{K}} \mu_2 p_k^{\text{u}}}_{\text{part 3}} \quad (14)$$

where

$$p_k^{\text{sec}} = \begin{cases} 1, & \text{if } R_k^{\text{sec}} < R_k^{\text{sec}, \min}, \forall k \in \mathcal{K}, \\ 0, & \text{otherwise,} \end{cases} \quad (15)$$

$$p_k^{\text{u}} = \begin{cases} 1, & \text{if } R_k < R_k^{\min}, \forall k \in \mathcal{K}, \\ 0, & \text{otherwise.} \end{cases} \quad (16)$$

In (14), the part 1 represents the immediate utility (system secrecy rate), the part 2 and the part 3 are the cost functions which are defined as the unsatisfied secrecy rate requirement and the unsatisfied minimum rate requirement, respectively. The coefficients  $\mu_1$  and  $\mu_2$  are the positive constants of the part 2 and the part 3 in (14), respectively, and they are used to balance the utility and cost [33]-[35].

The goals of (15) and (16) are to impose the QoS satisfaction levels of both the secrecy rate and the minimum data rate requirements, respectively. If the QoS requirement is satisfied in the current time slot, then  $p_k^{\text{sec}} = 0$  or  $p_k^{\text{u}} = 0$ , indicating that there is no punishment of the reward function due to the successful QoS guarantees.

The goal of the learning agent is to search for an optimal policy  $\pi^*$  ( $\pi$  is a mapping from states in  $\mathcal{S}$  to the probabilities of choosing an action in  $\mathcal{A}$ :  $\pi(s) : \mathcal{S} \rightarrow \mathcal{A}$ ) that maximizes the long-term expected discounted reward, and the cumulative discounted reward function can be defined as

$$U_t = \sum_{\tau=0}^{\infty} \gamma^\tau r_{t+\tau+1} \quad (17)$$

where  $\gamma \in (0, 1]$  denotes the discount factor. Under a certain policy  $\pi$ , the state-action function of the agent with a state-action pair  $(s, a)$  is given by

$$Q^\pi(s_t, a_t) = \mathbb{E}_\pi [U_t | s_t = s, a_t = a]. \quad (18)$$

The conventional Q-Learning algorithm can be adopted to learn the optimal policy. The key objective of Q-Learning is to update Q-table by using the Bellman's equation as follows:

$$Q^\pi(s_t, a_t) = \mathbb{E}_\pi \left[ r_t + \gamma \sum_{s_{t+1} \in \mathcal{S}} \mathcal{T}(s_{t+1} | s_t, a_t) \sum_{a_{t+1} \in \mathcal{A}} \pi(s_{t+1}, a_{t+1}) Q^\pi(s_{t+1}, a_{t+1}) \right] \quad (19)$$

The optimal action-value function in (17) is equivalent to the Bellman optimality equation, which is expressed by

$$Q^*(s_t, a_t) = r_t + \gamma \max_{a_{t+1}} Q^*(s_{t+1}, a_{t+1}) \quad (20)$$

and the state-value function is achieved as follows:

$$V(s_t) = \max_{a_t \in \mathcal{A}} Q(s_t, a_t). \quad (21)$$

In addition, the Q-value is updated as follows:

$$Q_{t+1}(s_t, a_t) = (1 - \alpha_t) Q_t(s_t, a_t) + \alpha_t (r_t + \gamma V_t(s_{t+1})) \quad (22)$$

where  $\alpha_t \in (0, 1]$  is the learning rate. Q-Learning generally constructs a lookup Q-table  $Q(s, a)$ , and the agent selects actions based on the greedy policy for each learning step [32]. In the  $\varepsilon$ -greedy policy, the agent chooses the action with the maximum Q-table value with probability  $1 - \varepsilon$ , whereas a random action is picked with probability  $\varepsilon$  to avoid achieving stuck at non-optimal policies [32]. Once the optimal Q-function  $Q^*(s, a)$  is achieved, the optimal policy is determined by

$$\pi^*(s, a) = \arg \max_{a \in \mathcal{A}} Q^*(s, a). \quad (23)$$

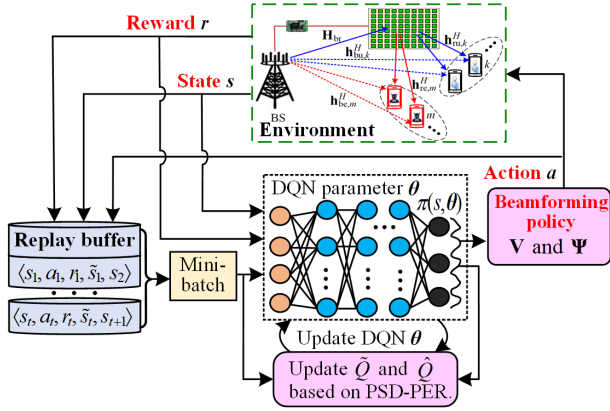


Fig. 2. Deep PDS-PER learning based beamforming for IRS-aided secure communications.

#### IV. DEEP PDS-PER LEARNING BASED SECURE BEAMFORMING

The secure beamforming policy discussed in Section III can be numerically achieved by using Q-Learning, policy gradient, and deep Q-Network (DQN) algorithms [32]. However, Q-Learning is not an efficient learning algorithm because it cannot deal with continuous state space and it has slow learning convergence speed. The policy gradient algorithm has the ability to handle continuous state-action spaces, but it may converge to a suboptimal solution. In addition, it is intractable for Q-learning and policy gradient algorithms to solve the optimization problem under high-dimensional input state space. Although DQN performs well in policy learning under high-dimensional state space, its non-linear Q-function estimator may lead to unstable learning process.

Considering the fact that the IRS-aided secure communication system has high-dimensional and high-dynamical characteristics according to the system state that is defined in (12) and uncertain CSI that is shown in (4) and (6), we propose a deep PDS-PER learning based secure beamforming approach, as shown in Fig. 2, where PDS-learning and PER mechanisms are utilized to enable the learning agent to learn and adapt faster in dynamic environments. In detail, the agent utilizes the observed state (i.e., CSI, previous secrecy rate, QoS satisfaction level), the feedback reward from environment as well as the historical experience from the replay buffer to train its learning model. After that, the agent employs the trained model to make decision (beamforming matrices  $\mathbf{V}$  and  $\mathbf{\Psi}$ ) based on its learned policy. The procedures of the proposed learning based secure beamforming are provided in the following subsections.

Note that the policy optimization (in terms of the BS's beamforming matrix  $\mathbf{V}$  and the RIS's reflecting beamforming matrix  $\mathbf{\Psi}$ ) in the IRS-aided secure communication system can be performed at the BS and that the optimized reflecting beamforming matrix can be transferred in an offline manner to the IRS by the controller to adjust the corresponding reflecting elements accordingly.

#### A. Proposed Deep PDS-PER Learning

As discussed in Section II, CSI is unlikely to be known accurately due to the transmission delay, processing delay, and mobility of users. At the same time, beamforming with outdated CSI will decrease the secrecy capacity, and therefore, a fast optimization solution needs to be designed to reduce processing delay. PDS-learning as a well-known algorithm has been used to improve the learning speed by exploiting extra partial information (e.g., the previous location information and the mobility velocity of MUs or eavesdroppers that affect the channel coefficients) and search for an optimized policy in dynamic environments [33]-[35]. Motivated by this, we devise a modified deep PDS-learning to trace the environment dynamic characteristics, and then adjust the transmit beamforming at the BS and the reflecting elements at the IRS accordingly, which can speed up the learning efficiency in dynamic environments.

PDS-learning can be defined as an immediate system state  $\tilde{s}_t \in \mathcal{S}$  happens after executing an action  $a_t$  at the current state  $s_t$  and before the next time state  $s_{t+1}$ . In detail, the PDS-learning agent takes an action  $a_t$  at state  $s_t$ , and then will receive known reward  $r^k(s_t, a_t)$  from the environment before transitioning the current state  $s_t$  to the PDS state  $\tilde{s}_t$  with a known transition probability  $\mathcal{T}^k(\tilde{s}_t|s_t, a_t)$ . After that, the PDS state further transform to the next state  $s_{t+1}$  with an unknown transition probability  $\mathcal{T}^u(s_{t+1}|\tilde{s}_t, a_t)$  and an unknown reward  $r^u(s_t, a_t)$ , which corresponds to the wireless CSI dynamics. In PDS-learning,  $s_{t+1}$  is independent of  $s_t$  given the PDS state  $\tilde{s}_t$ , and the reward  $r(s_t, a_t)$  is decomposed into the sum of  $r^k(s_t, a_t)$  and  $r^u(s_t, a_t)$  at  $\tilde{s}_t$  and  $s_{t+1}$ , respectively. Mathematically, the state transition probability in PDS-learning from  $s_t$  to  $s_{t+1}$  admits

$$\mathcal{T}(s_{t+1}|s_t, a_t) = \sum_{\tilde{s}_t} \mathcal{T}^u(s_{t+1}|\tilde{s}_t, a_t)\mathcal{T}^k(\tilde{s}_t|s_t, a_t). \quad (24)$$

Moreover, it can be verified that the reward of the current state-action pair  $(s_t, a_t)$  is expressed by

$$r(s_t, a_t) = r^k(s_t, a_t) + \sum_{\tilde{s}_t} \mathcal{T}^k(\tilde{s}_t|s_t, a_t)r^u(\tilde{s}_t, a_t). \quad (25)$$

At the time slot  $t$ , the PDS action-value function  $\tilde{Q}(\tilde{s}_t, a_t)$  of the current PDS state-action pair  $(\tilde{s}_t, a_t)$  is defined as

$$\tilde{Q}(\tilde{s}_t, a_t) = r^u(\tilde{s}_t, a_t) + \gamma \sum_{s_{t+1}} \mathcal{T}^u(s_{t+1}|\tilde{s}_t, a_t)V(s_{t+1}). \quad (26)$$

By employing the extra information (the known transition probability  $\mathcal{T}^k(\tilde{s}_t|s_t, a_t)$  and known reward  $r^k(s_t, a_t)$ ), the Q-function  $\hat{Q}(s_t, a_t)$  in PDS-learning can be further expanded under all state-action pairs  $(s, a)$ , which is expressed by

$$\hat{Q}(s_t, a_t) = r^k(s_t, a_t) + \sum_{\tilde{s}_t} \mathcal{T}^k(\tilde{s}_t|s_t, a_t)\tilde{Q}(\tilde{s}_t, a_t). \quad (27)$$

The state-value function in PDS-learning is defined by

$$\hat{V}_t(s_t) = \sum_{s_{t+1}} \mathcal{T}^k(s_{t+1}|s_t, a_t)\tilde{V}(s_{t+1}) \quad (28)$$

where  $\tilde{V}_t(s_{t+1}) = \max_{a_t \in \mathcal{A}} \tilde{Q}_t(s_{t+1}, a_t)$ . At each time slot, the PDS action-value function  $\tilde{Q}(\tilde{s}_t, a_t)$  is updated by

$$\begin{aligned} \tilde{Q}_{t+1}(\tilde{s}_t, a_t) &= (1 - \alpha_t)\tilde{Q}_t(\tilde{s}_t, a_t) \\ &\quad + \alpha_t \left( r^u(\tilde{s}_t, a_t) + \gamma \hat{V}_t(s_{t+1}) \right) \end{aligned} \quad (29)$$

After updating  $\tilde{Q}_{t+1}(\tilde{s}_t, a_t)$ , the action-value function  $\hat{Q}_{t+1}(s_t, a_t)$  can be updated by plugging  $\tilde{Q}_{t+1}(\tilde{s}_t, a_t)$  into (27).

After presenting in the above modified PDS-learning, a deep PDS learning algorithm is presented. In the presented learning algorithm, the traditional DQN is adopted to estimate the action-value Q-function  $Q(s, a)$  by using  $Q(s, a; \theta)$ , where  $\theta$  denote the DNN parameter. The objective of DQN is to minimize the following loss function at each time slot

$$\mathcal{L}(\theta_t) = \left[ \hat{V}_t(s_t; \theta_t) - \hat{Q}(s_t, a_t; \theta_t) \right]^2 = \left[ \{r(s_t, a_t) + \gamma \max_{a_{t+1} \in \mathcal{A}} \hat{Q}_t(s_{t+1}, a_{t+1}; \theta_t) - \hat{Q}(s_t, a_t; \theta_t)\}^2 \right] \quad (30)$$

where  $\hat{V}_t(s_t; \theta_t) = r(s_t, a_t) + \gamma \max_{a_{t+1} \in \mathcal{A}} \hat{Q}_t(s_{t+1}, a_{t+1}; \theta_t)$  is the target value. The error between  $\hat{V}_t(s_t; \theta_t)$  and the estimated value  $\hat{Q}(s_t, a_t; \theta_t)$  is usually called temporal-difference (TD) error, which is expressed by

$$\delta_t = \hat{V}_t(s_t; \theta_t) - \hat{Q}(s_t, a_t; \theta_t). \quad (31)$$

The DNN parameter  $\theta$  is achieved by taking the partial differentiation of the objective function (30) with respect to  $\theta$ , which is given by

$$\theta_{t+1} = \theta_t + \beta \nabla \mathcal{L}(\theta_t). \quad (32)$$

where  $\beta$  is the learning rate of  $\theta$ , and  $\nabla(\cdot)$  denotes the first-order partial derivative.

Accordingly, the policy  $\hat{\pi}_t(s)$  of the modified deep PDS-learning algorithm is given by

$$\hat{\pi}_t(s) = \arg \max_{a_t \in \mathcal{A}} \hat{Q}(s_t, a_t; \theta_t). \quad (33)$$

Although DQN is capable of performing well in policy learning with continuous and high-dimensional state space, DNN may learn ineffectively and cause divergence owing to the nonstationary targets and correlations between samples. Experience replay is utilized to avoid the divergence of the RL algorithm. However, classical DQN uniformly samples each transition  $e_t = \langle s_t, a_t, r_t, \tilde{s}_t, s_{t+1} \rangle$  from the experience replay, which may lead to an uncertain or negative effect on learning a better policy. The reason is that different transitions (experience information) in the replay buffer have different importance for the learning policy, and sampling every transition equally may unavoidably result in inefficient usage of meaningful transitions. Therefore, a prioritized experience replay (PER) scheme has been presented to address this issue and enhance the sampling efficiency [36], [37], where the priority of transition is determined by the values of TD error. In PER, a transition with higher absolute TD error has higher priority in the sense that it has more aggressive correction for the action-value function.

In the deep PDS-PER learning algorithm, similar to classical DQN, the agent collects and stores each experience  $e_t = \langle s_t, a_t, r_t, \tilde{s}_t, s_{t+1} \rangle$  into its experience replay buffer, and DNN updates the parameter by sampling a mini-batch of tuples from the replay buffer. So far, PER was adopted only for DRL

and Q-learning, and has never been employed with the PDS-learning algorithm to learn the dynamic information. In this paper, we further extend this PER scheme to enable prioritized experience replay in the proposed deep PDS-PER learning framework, in order to improve the learning convergence rate.

The probability of sampling transition  $i$  (experience  $i$ ) based on the absolute TD-error is defined by

$$p(i) = |\delta(i)|^{\eta_1} / \sum_{j'} |\delta(j')|^{\eta_1} \quad (34)$$

where the exponent  $\eta_1$  weights how much prioritization is used, with  $\eta_1 = 0$  corresponding to being uniform sampling. The transition with higher  $p(i)$  will be more likely to be replayed from the replay buffer, which is associated with very successful attempts by preventing the DNN from being over-fitting. With the help of PER, the proposed deep PDS-PER learning algorithm tends to replay valuable experience and hence learns more effectively to find the best policy.

It is worth noting that experiences with high absolute TD-error are more frequently replayed, which alters the visitation frequency of some experiences and hence causes the training process of the DNN prone to diverge. To address this problem, importance-sampling (IS) weights are adopted in the calculation of weight changes

$$W(i) = (D \cdot p(i))^{-\eta_2} \quad (35)$$

where  $D$  is the size of the experience replay buffer, and the parameter  $\eta_2$  is used to adjust the amount of correction used.

Accordingly, by using the PER scheme into the deep PDS-PER learning, the DNN loss function (30) and the corresponding parameters are rewritten respectively as follows:

$$\mathcal{L}(\theta_t) = \frac{1}{H} \sum_{i=1}^H (W_i \mathcal{L}_i(\theta_t)) \quad (36)$$

$$\theta_{t+1} = \theta_t + \beta \delta_t \nabla_{\theta} \mathcal{L}(\theta_t) \quad (37)$$

*Theorem 1:* The presented deep PDS-PER learning can converge to the optimal  $\hat{Q}(s_t, a_t)$  of the MDP with probability 1 when the learning rate sequence  $\alpha_t$  meets the following conditions  $\alpha_t \in [0, 1)$ ,  $\sum_{t=0}^{\infty} \alpha_t = \infty$  and  $\sum_{t=0}^{\infty} \alpha_t^2 < \infty$ , where the aforementioned requirements have been appeared in most of the RL algorithms [32] and they are not specific to the proposed deep PDS-PER learning algorithm [32].

*Proof:* If each action can be executed with an infinite number of learning steps at each system state, or in other words, the learning policy is greedy with the infinite explorations, the Q-function  $\hat{Q}(s_t, a_t)$  in PDS-learning and its corresponding policy strategy  $\pi(s)$  will converge to the optimal points, respectively, with probability of 1 [33]-[35]. The existing references [34] and [35] have provided the proof.

### B. Secure Beamforming Based on Proposed Deep PDS-PER Learning

Similar to most DRL algorithms, our proposed deep PDS-PER learning based secure beamforming approach consists of two stages, i.e., the training stage and implementation stage. The training process of the proposed approach is shown in

**Algorithm 1.** A central controller at the BS is responsible for collecting environment information and making decision for secure beamforming.

In the training stage, similar to RL-based policy control, the controller initializes network parameters and observes the current system state including CSI of all users, the previous predicted secrecy rate and the transmission data rate. Then, the state vector is input into DQN to train the learning model. The  $\epsilon$ -greedy scheme is leveraged to balance both the exploration and exploitation, i.e., the action with the maximum reward is selected probability  $1 - \epsilon$  according to the current information (exploitation, which is known knowledge), while a random action is chosen with probability  $\epsilon$  based on the unknown knowledge (i.e., keep trying new actions, hoping it brings even higher reward (exploration, which is unknown knowledge)). After executing the selected action, the agent receives a reward from the environment and observes the state transition from  $s_t$  to PDS state  $\tilde{s}_t$  and then to the next state  $s_{t+1}$ . Then, PDS-learning is used to update the PDS action-value function  $\tilde{Q}(\tilde{s}_t, a_t; \theta_t)$  and Q-function  $\hat{Q}(s_t, a_t; \theta_t)$ , before collecting and storing the transition tuple (also called experience)  $e_t = \langle s_t, a_t, r_t, \tilde{s}_t, s_{t+1} \rangle$  into the experience replay memory buffer  $\mathcal{D}$ , which includes the current system state, selected action, instantaneous reward and PDS state along with the next state. The experience in the replay buffer is selected by the PER scheme to generate mini-batches and they are used to train DQN. In detail, the priority of each transition  $p(i)$  is calculated by using (34) and then get its IS weight  $W(i)$  in (35), where the priorities ensure that high-TD-value ( $\delta(i)$ ) transitions are replayed more frequently. The weight  $W(i)$  is integrated into deep PDS learning to update both the loss function  $\mathcal{L}(\theta)$  and DNN parameter  $\theta$ . Once DQN converges, the deep PDS-PER learning model is achieved.

After adequate training in **Algorithm 1**, the learning model is loaded for the implementation stage. During the implementation stage, the controller uses the trained learning model to output its selected action  $a$  by going through the DNN parameter  $\theta$ , with the observed state  $s$  from the IRS-aided secure communication system. Specifically, it chooses an action  $a$ , with the maximum value based on the trained deep PDS-PER learning model. Afterwards, the environment feeds back an instantaneous reward and a new system state to the agent. Finally, the beamforming matrix  $\mathbf{V}^*$  at the BS and the phase shift matrix  $\Psi^*$  (reflecting beamforming) at the IRS are achieved according to the selected action.

We would like to point out that the training stage needs a powerful computation server which can be performed offline at the BS while the implementation stage can be completed online. The trained learning model requires to be updated only when the environment (IRS-aided secure communication system) has experienced greatly changes, mainly depending on the environment dynamics and service requirements.

### C. Computational Complexity Analysis

For the training stage, in DNN, let  $L$ ,  $Z_0$  and  $Z_l$  denote the training layers, the size of the input layer (which is proportional to the number of states) and the number of neurons in

### Algorithm 1 Deep PDS-PER Learning Based Secure Beamforming

---

1: **Input:** IRS-aided secure communication simulator and QoS requirements of all MUs (e.g., minimum secrecy rate and transmission rate).  
2: **Initialize:** DQN with initial Q-function  $Q(s, a; \theta)$ , parameters  $\theta$ , learning rate  $\alpha$  and  $\beta$ .  
3: **Initialize:** experience replay buffer  $\mathcal{D}$  with size  $D$ , and mini-batch size  $H$ .  
4: **for** each episode  $= 1, 2, \dots, N^{\text{epi}}$  **do**  
5:   Observe an initial system state  $s$ ;  
6:   **for** each time step  $t=0, 1, 2, \dots, T$  **do**  
7:     Select action based on the  $\epsilon$ -greedy policy at current state  $s_t$ :  
   choose a random action  $a_t$  with probability  $\epsilon$ ;  
8:     Otherwise,  $a_t = \arg \max_{a_t \in \mathcal{A}} Q(s_t, a_t; \theta_t)$ ;  
9:     Execute action  $a_t$ , receive an immediate reward  $r^k(s_t, a_t)$  and observe the state transition from  $s_t$  to PDS state  $\tilde{s}_t$  and then to the next state  $s_{t+1}$ ;  
10:     Update the reward function  $r(s_t, a_t)$  under PDS-learning using (25);  
11:     Update the PDS action-value function  $\tilde{Q}(\tilde{s}_t, a_t; \theta_t)$  using (29);  
12:     Update the Q-function  $\hat{Q}(s_t, a_t; \theta_t)$  using (25);  
13:     Store PDS experience  $e_t = \langle s_t, a_t, r_t, \tilde{s}_t, s_{t+1} \rangle$  in experience replay buffer  $\mathcal{D}$ , if  $\mathcal{D}$  is full, remove least used experience from  $\mathcal{D}$ ;  
14:     **for**  $i = 1, 2, \dots, H$  **do**  
15:       Sample transition  $i$  with the probability  $p(i)$  using (34);  
16:       Calculate the absolute TD-error  $|\delta(i)|$  in (31);  
17:       Update the corresponding IS weight  $W_i$  using (35);  
18:       Update the priority of transition  $i$  based on  $|\delta(i)|$ ;  
19:     **end for**  
20:     Update the loss function  $\mathcal{L}(\theta)$  and parameter  $\theta$  of DQN using (36) and (37), respectively;  
21:   **end for**  
22: **end for**  
23: **Output:** Return the deep PDS-PER learning model.

---

the  $l$ -th layer, respectively. The computational complexity in each time step for the agent is  $O(Z_0 Z_l + \sum_{l=1}^{L-1} Z_l Z_{l+1})$ . In the training phase, each mini-batch has  $N^{\text{epi}}$  episodes with each episode being  $T$  time steps, each trained model is completed iteratively until convergence. Hence, the total computational complexity in DNN is  $O(N^{\text{epi}} T (Z_0 Z_l + \sum_{l=1}^{L-1} Z_l Z_{l+1}))$ . The high computational complexity of the DNN training phase can be performed offline for a finite number of episodes at a centralized powerful unit (such as the BS).

In our proposed deep PDS-PER learning algorithm, PDS-learning and PER schemes are utilized to improve the learning efficiency and enhance the convergence speed, which requires extra computational complexity. In PDS-learning learning, since the set of PDS states is the same as the set of MDP states  $\mathcal{S}$  [30]-[32], the computational complexity of the classical DQN algorithm and the deep PDS-learning algorithm are  $O(|\mathcal{S}|^2 \times |\mathcal{A}|)$  and  $O(2|\mathcal{S}|^2 \times |\mathcal{A}|)$ , respectively. In PER, since the relay buffer size is  $D$ , the system requires to make both updating and sampling  $O(\log_2 D)$  operations, so the computational complexity of the PER scheme is  $O(\log_2 D)$ .

According the above analysis, the complexity of the classical DQN algorithm and the proposed deep PDS-PER learning algorithm are respectively

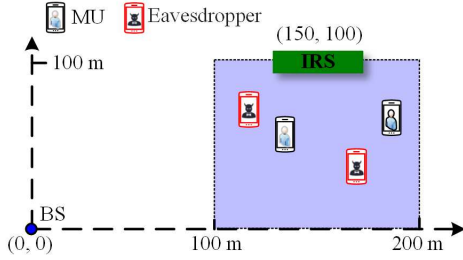


Fig. 3. Simulation setup.

$O\left( IN^{\text{epiT}}(Z_0 Z_l + \sum_{i=1}^{L-1} Z_i Z_{i+1}) + |S|^2 \times |A| \right)$  and  $O\left( IN^{\text{epiT}}(Z_0 Z_l + \sum_{i=1}^{L-1} Z_i Z_{i+1}) + 2|S|^2 \times |A| + \log_2 D \right)$ , indicating that the complexity of the proposed algorithm is slightly higher than the classical DQN learning algorithm. However, our proposed algorithm achieves better performance than that of the classical DQN algorithm, which will be shown in the next section.

#### D. Implementation Details of DRL

This subsection provides extensive details regarding the generation of training, validation, and testing dataset production.

**Generation of training:** As shown in Fig. 3,  $K$  single-antenna MUs and  $M$  single-antenna eavesdroppers are randomly located in the  $100\text{m} \times 100\text{m}$  half right-hand side rectangular of Fig. 3 (light blue area) in a two-dimensional x-y rectangular grid plane. The BS and the IRS are located at  $(0, 0)$  and  $(150, 100)$  in meter (m), respectively. The x-y grid has dimensions  $100\text{m} \times 100\text{m}$  with a resolution of 2.5 m, i.e., a total of 1600 points.

In the presented IRS-assisted system, the system beamforming codebook  $\mathcal{F}$  includes the BS's beamforming codebook  $\mathcal{F}_{\text{BS}}$  and the IRS's beamforming codebook  $\mathcal{F}_{\text{IRS}}$ . Both the BS's beamforming matrix  $\mathbf{V}$  and the IRS's reflection beamforming matrix  $\Psi$  are picked from the pre-defined codebook  $\mathcal{F}_{\text{BS}}$  and  $\mathcal{F}_{\text{IRS}}$ , respectively. The data points of sampled channel vector and the corresponding reward vector  $\langle \mathbf{h}, \mathbf{r} \rangle$  is added into the DNN training data set  $\mathcal{D}$ . The sampled channel,  $\mathbf{h}$ , is the input to DQN. All the samples are normalized by using the normalization scheme to realize a simple per-dataset scaling. After training, the selected BS's beamforming matrix  $\mathbf{V}$  and IRS's beamforming matrix  $\Psi$  with the highest achievable reward are used to reflect the security communication performance.

The DQN learning model is trained using empirically hyperparameter, where DNN trained for 1000 epochs with 128 mini-batches being utilized in each epoch. In the training process, 80% and 20% of all generated data are selected as the training and validation (test) datasets, respectively. The experience replay buffer size is 32000 where the corresponding samples are randomly sampled from this number of the most recently experiences.

**DQN structure:** The DQN model is designed as a Multi-Layer Perceptron network, which is also referred to as the feedforward Fully Connected network. Note here that Multi-Layer Perceptron network is widely used to build an advanced

estimator, which fulfills the relation between the environment descriptors and the beamforming matrices (both the BS's beamforming matrix and the IRS's reflecting beamforming matrix).

The DQN model is comprised of  $L$  layers, as illustrated in Fig. 2, where the first layer is input layer, the last layer is output layer and the remaining layers are the hidden layers. The  $l$ -th hidden layer in the network has a stack of neurons, each of which connects all the outputs of the previous layer. Each unit operates on a single input value outputting another single value. The input of the input layer consist of the systems states, i.e., channel samples, the achievable rate and QoS satisfaction level information in the last time slot, while the output layer outputs the predicted reward values with beamforming matrices in terms of the BS's beamforming matrix and the IRS's reflecting beamforming matrix. The DQN construction is used for training stability. The network parameters will be provided in the next section.

**Training loss function:** The objective of DRL model is to find the best beamforming matrices, i.e.,  $\mathbf{V}$  and  $\Psi$ , from the beamforming codebook with the highest achievable reward from the environment. In this case, having the highest achievable reward estimation, the regression loss function is adopted to train the learning model, where DNN is trained to make its output,  $\hat{\mathbf{r}}$ , as close as possible to the desired normalized reward,  $\bar{\mathbf{r}}$ . Formally, the training is driven by minimizing the loss function,  $\mathcal{L}(\theta)$ , defined as

$$\mathcal{L}(\theta) = \text{MSE}(\hat{\mathbf{r}}, \bar{\mathbf{r}}), \quad (38)$$

where  $\theta$  is the set of all DNN parameters,  $\text{MSE}(\cdot)$  denotes the mean-squared-error between  $\hat{\mathbf{r}}$  and  $\bar{\mathbf{r}}$ . Note that the outputs of DNN,  $\hat{\mathbf{r}}$  can be acted as functions of  $\theta$  and the inputs of DNN are the system states shown in (12) in the paper.

## V. SIMULATION RESULTS AND ANALYSIS

This section evaluates the performance of the IRS-aided secure communication system. The background noise power of MUs and eavesdroppers is equal to -90 dBm. We set the number of antennas at the BS is  $N = 4$ , the number of MUs is  $K = 2$  and the number of eavesdroppers is  $M = 2$ . The transmit power  $P_{\text{max}}$  at the BS varies between 15 dBm and 40 dBm, the number of IRS elements  $L$  varies between 10 and 60, and the outdated CSI coefficient  $\rho$  varies from 0.5 to 1 for different simulation settings. The minimum secrecy rate and the minimum transmission data rate are 3 bits/s/Hz and 5 bits/s/Hz, respectively. The path loss model is defined by  $PL = (PL_0 - 10\zeta \log_{10}(d/d_0))$  dB, where  $PL_0 = 30$  dB is the path loss at the reference distance  $d_0 = 1$  m [9], [38],  $\zeta = 3$  is the path loss exponent, and  $d$  is the distance from the transmitter to the receiver. The learning model consists of three connected hidden layers, containing 500, 250, and 200 neurons [39], respectively. The learning rate is set to  $\alpha = 0.002$  and the discount factor is set to  $\gamma = 0.95$ . The exploration rate  $\varepsilon$  is linearly annealed from 0.8 to 0.1 over the beginning 300 episodes and remains constant afterwards. The parameters  $\mu_1$  and  $\mu_2$  in (12) are set to  $\mu_1 = \mu_2 = 2$  to balance the utility and cost [33]-[35]. Similar to the IRS-aided communication



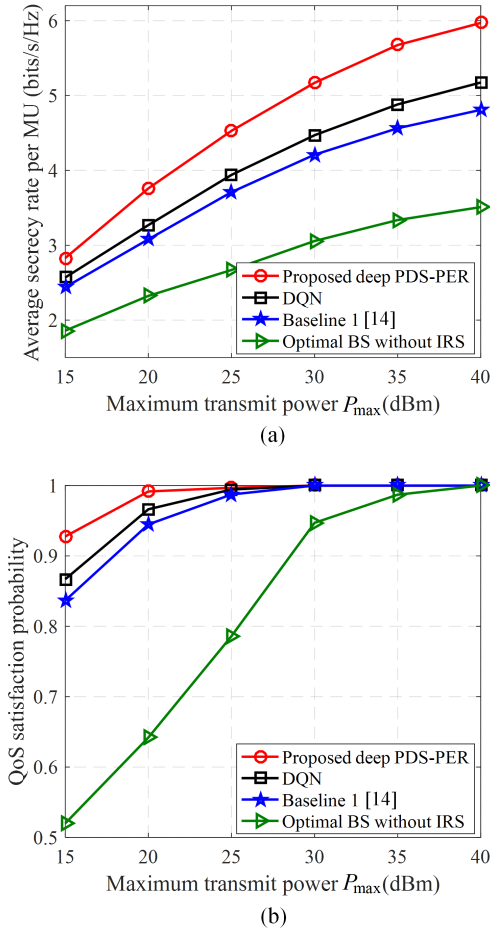


Fig. 6. Performance comparisons versus the maximum transmit power at the BS.

monotonically with increasing  $P_{\max}$ . The reason is that when  $P_{\max}$  increases, the received SINR at MUs improves, leading to the performance improvement. In addition, we find that our proposed learning approach outperforms the Baseline1 approach. In fact, our approach jointly optimizes the beamforming matrixes  $\mathbf{V}$  and  $\mathbf{\Psi}$ , which can simultaneously facilitates more favorable channel propagation benefit for MUs and impair eavesdroppers, while the Baseline1 approach optimizes the beamforming matrixes in an iterative way. Moreover, our proposed approach has higher performance than DQN in terms of both secrecy rate and QoS satisfaction probability, due to its efficient learning capacity by utilizing PDS-learning and PER schemes in the dynamic environment. From Fig. 6, we also find that the three IRS assisted secure beamforming approaches provide significant higher secrecy rate and QoS satisfaction probability than the traditional system without IRS. This indicates that the IRS can effectively guarantee secure communication and QoS requirements via reflecting beamforming, where reflecting elements (IRS-induced phases) at the IRS can be adjusted to maximize the received SINR at MUs and suppress the wiretapped rate at eavesdroppers.

In Fig. 7, the achievable secrecy rate and QoS satisfaction level performance of all approaches are evaluated through changing the IRS elements, i.e., from  $L = 10$  to 60, when

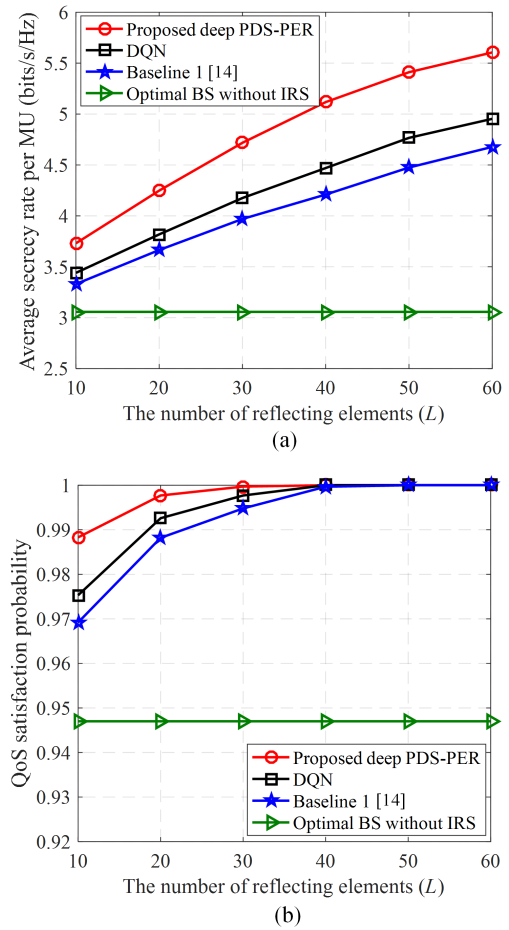


Fig. 7. Performance comparisons versus the number of IRS elements.

$P_{\max} = 30$  dBm and  $\rho = 0.95$ . For the secure beamforming approaches assisted by the IRS, their achievable secrecy rates and QoS satisfaction levels significantly increase with the number of the IRS elements. The improvement results from the fact that more IRS elements, more signal paths and signal power can be reflected by the IRS to improve the received SINR at the MUs but to decrease the received SINR at the eavesdroppers. In addition, the performance of the approach without IRS remains constant under the different numbers of the IRS elements.

From Fig. 7(a), it is found that the secrecy rate of the proposed learning approach is higher than those of the Baseline 1 and DQN approaches, especially, their performance gap also obviously increases with  $L$ , this is because that with more reflecting elements at the IRS, the proposed deep PDS-PER learning based secure communication approach becomes more flexible for optimal phase shift (reflecting beamforming) design and hence achieves higher gains. In addition, from Fig. 7(b) compared with the Baseline 1 and DQN approaches, as the reflecting elements at the IRS increases, we observe that the proposed learning approach is the first one who attains 100% QoS satisfaction level. This superior achievements are based on the particular design of the QoS-aware reward function shown in (14) for secure communication.

In Fig. 8, we further analyze how the system secrecy rate

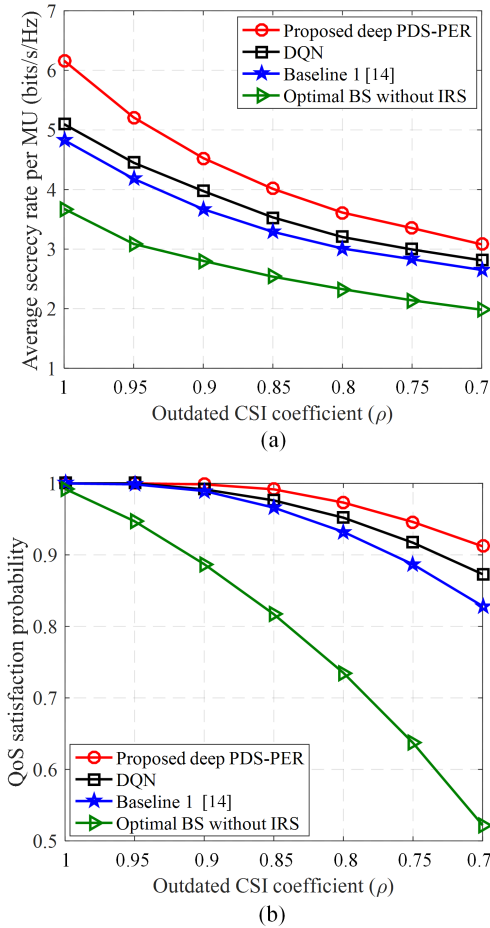


Fig. 8. Performance comparisons versus outdated CSI coefficient  $\rho$ .

and QoS satisfaction level performances are affected by the outdated CSI coefficient  $\rho$  in the system, i.e., from  $\rho = 0.5$  to 1, when  $P_{\max} = 30$  dBm and  $L = 40$ . Note that as  $\rho$  decreases, the CSI becomes more outdated as shown in (4) and (6), and  $\rho = 1$  means non-outdated CSI. It can be observed from all beamforming approaches, when CSI becomes more outdated (as  $\rho$  decreases), the average secrecy rate and QoS satisfaction level decrease. The reason is that a higher value of  $\rho$  indicates more accurate CSI, which will enable all the approaches to optimize secure beamforming policy to achieve higher average secrecy rate and QoS satisfaction level in the system.

It can be observed that reducing  $\rho$  has more effects on the performance of the other three approaches while our proposed learning approach still maintains the performance at a favorable level, indicating that the other three approaches are more sensitive to the uncertainty of CSI and the robust of the proposed learning approach. For instance, the proposed learning approach achieves the secrecy rate and QoS satisfaction level improvements of 17.21% and 8.67%, compared with the Baseline 1 approach when  $\rho = 0.7$ . Moreover, in comparison, the proposed learning approach achieves the best performance among all approaches against channel uncertainty. The reason is that the proposed learning approach considers the time-

varying channels and takes advantage of PDS-learning to effectively learn the dynamic environment.

## VI. CONCLUSION

In this work, we have investigated the joint BS's beamforming and IRS's reflect beamforming optimization problem under the time-varying channel conditions. As the system is highly dynamic and complex, we have exploited the recent advances of machine learning, and formulated the secure beamforming optimization problem as an RL problem. A deep PDS-PER learning based secure beamforming approach has been proposed to jointly optimize both the BS's beamforming and the IRS's reflect beamforming in the dynamic IRS-aided secure communication system, where PDS and PER schemes have been utilized to improve the learning convergence rate and efficiency. Simulation results have verified that the proposed learning approach outperforms other existing approaches in terms of enhancing the system secrecy rate and the QoS satisfaction probability.

## REFERENCES

- [1] N. Yang, L. Wang, G. Geraci, M. Elkashlan, J. Yuan, and M. D. Renzo, "Safeguarding 5G wireless communication networks using physical layer security," *IEEE Commun. Mag.*, vol. 53, no. 4, pp. 20-27, Apr. 2015.
- [2] A. D. Wyner, "The wiretap channel," *Bell Syst. Tech. J.*, vol. 54, no. 8, pp. 1355-1387, Oct. 1975.
- [3] Q. Li and L. Yang, "Beamforming for cooperative secure transmission in cognitive two-way relay networks," *IEEE Trans. Inf. Forensics Security*, vol. 15, pp. 130-143, Jan. 2020.
- [4] L. Xiao, X. Lu, D. Xu, Y. Tang, L. Wang, and W. Zhuang, "UAV relay in VANETs against smart jamming with reinforcement learning," *IEEE Trans. Veh. Technol.*, vol. 67, no. 5, pp. 4087-4097, May 2018.
- [5] W. Wang, K. C. Teh and K. H. Li, "Artificial noise aided physical layer security in multi-antenna small-cell networks," *IEEE Trans. Inf. Forensics Security*, vol. 12, no. 6, pp. 1470-1482, Jun. 2017.
- [6] H. Wang, T. Zheng, and X. Xia, "Secure MISO wiretap channels with multiantenna passive eavesdropper: Artificial noise vs. artificial fast fading," *IEEE Trans. Wireless Commun.*, vol. 14, no. 1, pp. 94-106, Jan. 2015.
- [7] R. Nakai and S. Sugiura, "Physical layer security in buffer-state-based max-ratio relay selection exploiting broadcasting with cooperative beamforming and jamming," *IEEE Trans. Inf. Forensics Security*, vol. 14, no. 2, pp. 431-444, Feb. 2019.
- [8] Z. Mobini, M. Mohammadi, and C. Tellambura, "Wireless-powered full-duplex relay and friendly jamming for secure cooperative communications," *IEEE Trans. Inf. Forensics Security*, vol. 14, no. 3, pp. 621-634, Mar. 2019.
- [9] Q. Wu and R. Zhang, "Towards smart and reconfigurable environment: Intelligent reflecting surface aided wireless network," *IEEE Commun. Mag.*, vol. 58, no. 1, pp. 106-112, Jan. 2020.
- [10] J. Zhao, "A survey of intelligent reflecting surfaces (IRSs): Towards 6G wireless communication networks," 2019. [Online]. Available: <https://arxiv.org/abs/1907.04789>.
- [11] H. Han, *et al.*, "Intelligent reflecting surface aided power control for physical-layer broadcasting," 2019. [Online]. Available: <https://arxiv.org/abs/1912.03468>.
- [12] C. Huang, A. Zappone, G. C. Alexandropoulos, M. Debbah, and C. Yuen, "Reconfigurable intelligent surfaces for energy efficiency in wireless communication," *IEEE Trans. Wireless Commun.*, vol. 18, no. 8, pp. 4157-4170, Aug. 2019.
- [13] Q. Wu and R. Zhang, "Intelligent reflecting surface enhanced wireless network via joint active and passive beamforming," *IEEE Trans. Wireless Commun.*, vol. 18, no. 11, pp. 5394-5409, Nov. 2019.
- [14] M. Cui, G. Zhang, and R. Zhang, "Secure wireless communication via intelligent reflecting surface," *IEEE Wireless Commun. Lett.*, vol. 8, no. 5, pp. 1410-1414, Oct. 2019.

[15] H. Shen, W. Xu, S. Gong, Z. He, and C. Zhao, "Secrecy rate maximization for intelligent reflecting surface assisted multi-antenna communications," *IEEE Commun. Lett.*, vol. 23, no. 9, pp. 1488-1492, Sep. 2019.

[16] X. Yu, D. Xu, and R. Schober, "Enabling secure wireless communications via intelligent reflecting surfaces," in *Proc. IEEE Global Commun. Conf. (GLOBECOM)*, Waikoloa, HI, USA, Dec. 2019, pp. 1-6

[17] Q. Wu and R. Zhang, "Beamforming optimization for wireless network aided by intelligent reflecting surface with discrete phase shifts," *IEEE Trans. Commun.*, vol. 68, no. 3, pp. 1838-1851, Mar. 2020.

[18] Z. Chu, W. Hao, P. Xiao, and J. Shi, "Intelligent reflecting surface aided multi-antenna secure transmission," *IEEE Wireless Commun. Lett.*, vol. 9, no. 1, pp. 108-112, Jan. 2020.

[19] B. Feng, Y. Wu, and M. Zheng, "Secure transmission strategy for intelligent reflecting surface enhanced wireless system," 2019. [Online]. Available: <http://arxiv.org/abs/1909.00629>.

[20] J. Chen, Y. Liang, Y. Pei and H. Guo, "Intelligent reflecting surface: A programmable wireless environment for physical layer security," *IEEE Access*, vol. 7, pp. 82599-82612, May 2019.

[21] X. Yu, D. Xu, Y. Sun, D. W. K. Ng, and R. Schober, "Robust and secure wireless communications via intelligent reflecting surfaces," 2019. [Online]. Available: <https://arxiv.org/abs/1912.01497>.

[22] X. Guan, Q. Wu, and R. Zhang, "Intelligent reflecting surface assisted secrecy communication: Is artificial noise helpful or not?," *IEEE Wireless Commun. Lett.*, vol. 9, no. 6, pp. 778-782, Jun. 2020.

[23] L. Dong and H. Wang, "Secure MIMO transmission via intelligent reflecting surface," *Appear in IEEE Wireless Commun. Lett.*, vol. 9, no. 6, pp. 787-790, June 2020.

[24] W. Jiang, Y. Zhang, J. Wu, W. Feng, and Y. Jin, "Intelligent reflecting surface assisted secure wireless communications with multiple-transmit and multiple-receive antennas," 2019. [Online]. Available: <https://arxiv.org/abs/2001.08963>.

[25] D. Xu, X. Yu, Y. Sun, D. W. K. Ng, and R. Schober, "Resource allocation for secure IRS-assisted multiuser MISO systems," 2019. [Online]. Available: <http://arxiv.org/abs/1907.03085>.

[26] C. Huang, G. C. Alexandropoulos, C. Yuen, and M. Debbah, "Indoor signal focusing with deep learning designed reconfigurable intelligent surfaces," 2019. [Online]. Available: <https://arxiv.org/abs/1905.07726>.

[27] A. Taha, M. Alrabeiah, and A. Alkhateeb, "Enabling large intelligent surfaces with compressive sensing and deep learning," 2019. [Online]. Available: <https://arxiv.org/abs/1904.10136>.

[28] K. Feng, Q. Wang, X. Li and C. Wen, "Deep reinforcement learning based intelligent reflecting surface optimization for MISO communication systems," *IEEE Wireless Commun. Lett.*, vol. 9, no. 5, pp. 745-749, May 2020.

[29] C. Huang, R. Mo, and C. Yuen, "Reconfigurable intelligent surface assisted multiuser MISO systems exploiting deep reinforcement learning," 2020. [Online]. Available: <https://arxiv.org/abs/2002.10072>.

[30] C. Li, W. Zhou, K. Yu, L. Fan, and J. Xia, "Enhanced secure transmission against intelligent attacks," *IEEE Access*, vol. 7, pp. 53596-53602, Aug. 2019.

[31] L. Xiao, G. Sheng, S. Liu, H. Dai, M. Peng, and J. Song, "Deep reinforcement learning-enabled secure visible light communication against eavesdropping," *IEEE Trans. Commun.*, vol. 67, no. 10, pp. 6994-7005, Oct. 2019.

[32] M. Wiering and M. Otterlo, *Reinforcement learning: State-of-the-art*, Springer Publishing Company, Incorporated, 2014.

[33] H. L. Yang A. Alphones, C. Chen, W. D. Zhong, and X. Z. Xie, "Learning-based energy-efficient resource management by heterogeneous RF/VLC for ultra-reliable low-latency industrial IoT networks," *IEEE Trans. Ind. Informat.*, vol. 16, no. 8, pp. 5565-5576, Aug. 2020.

[34] X. He, R. Jin, and H. Dai, "Deep PDS-learning for privacy-aware offloading in MEC-enabled IoT," *IEEE Internet of Things J.*, vol. 6, no. 3, pp. 4547-4555, Jun. 2019

[35] N. Mastrorade and M. van der Schaar, "Joint physical-layer and system-level power management for delay-sensitive wireless communications," *IEEE Trans. Mobile Comput.*, vol. 12, no. 4, pp. 694-709, Apr. 2013.

[36] T. Schaul, J. Quan, I. Antonoglou, and D. Silver, "Prioritized experience replay," in *Proc. 4th Int. Conf. Learn. Represent. (ICLR)*, San Juan, US, May. 2016, pp. 1-21.

[37] H. Gacanin and M. Di Renzo, "Wireless 2.0: Towards an intelligent radio environment empowered by reconfigurable metasurfaces and artificial intelligence," 2020. [Online]. Available: <https://arxiv.org/abs/2002.11040>.

[38] C. W. Huang, *et al.*, "Holographic MIMO surfaces for 6G wireless networks: opportunities, challenges, and trends," to appear in *IEEE Wireless Commun.*, Apr. 2020.

[39] F. B. Mismar, B. L. Evans, and A. Alkhateeb, "Deep reinforcement learning for 5G networks: Joint beamforming, power control, and interference coordination," *IEEE Trans. Commun.*, vol. 68, no. 3, pp. 1581-1592, Mar. 2020.

[40] H. Yang, *et al.*, "Deep reinforcement learning based intelligent reflecting surface for secure wireless communications," will be presented in *Proc. IEEE Global Commun. Conf. (GLOBECOM)*, Dec. 2020, Taipei, Taiwan.



**Helin Yang** (S'15) received the B.S. and M.S. degrees in the School of Telecommunications Information Engineering from Chongqing University of Posts and Telecommunications in 2013, and 2016, and the Ph.D. degree from School of Electrical and Electronic Engineering, Nanyang Technological University, Singapore, in 2020. His current research interests include wireless communication, visible light communication, Internet of Things and resource management.



**Zehui Xiong** (S'17) is currently a researcher with Alibaba-NTU Singapore Joint Research Institute, Nanyang Technological University, Singapore. He received the Ph.D. degree at Nanyang Technological University, Singapore. He received the B.Eng degree with the highest honors at Huazhong University of Science and Technology, Wuhan, China. He is the visiting scholar with Princeton University and University of Waterloo. His research interests include network economics, wireless communications, blockchain, and edge intelligence. He has published more than 60 peer-reviewed research papers in leading journals and flagship conferences, and 3 of them are ESI Highly Cited Papers. He has won several Best Paper Awards. He is an Editor for Elsevier Computer Networks (COMNET) and Elsevier Physical Communication (PHYCOM), and an Associate Editor for IET Communications. He is the recipient of the Chinese Government Award for Outstanding Students Abroad in 2019, and NTU SCSE Outstanding PhD Thesis Runner-Up Award in 2020.

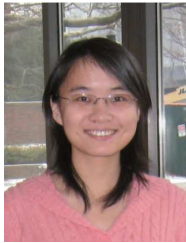


**Jun Zhao** (S'10-M'15) is currently an Assistant Professor in the School of Computer Science and Engineering at Nanyang Technological University (NTU) in Singapore. He received a PhD degree in Electrical and Computer Engineering from Carnegie Mellon University (CMU) in the USA (advisors: Virgil Gligor, Osman Yagan; collaborator: Adrian Perrig), affiliating with CMU's renowned CyLab Security & Privacy Institute, and a bachelor's degree from Shanghai Jiao Tong University in China. Before joining NTU first as a postdoc with Xiaokui

Xiao and then as a faculty member, he was a postdoc at Arizona State University as an Arizona Computing PostDoc Best Practices Fellow (advisors: Junshan Zhang, Vincent Poor). His research interests include communications, networks, security, and AI.

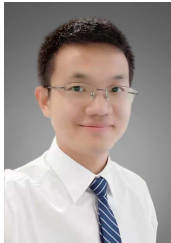


**Dusit Niyato** (M'09-SM'15-F'17) is currently a professor in the School of Computer Science and Engineering, at Nanyang Technological University, Singapore. He received B.Eng. from King Mongkuts Institute of Technology Ladkrabang (KMUTL), Thailand in 1999 and Ph.D. in Electrical and Computer Engineering from the University of Manitoba, Canada in 2008. His research interests are in the area of energy harvesting for wireless communication, Internet of Things (IoT) and sensor networks.



**Liang Xiao** (M'09-SM'13) is currently a Professor in the Department of Information and Communication Engineering, Xiamen University, Xiamen, China. She has served as an associate editor of IEEE Trans. Information Forensics and Security and guest editor of IEEE Journal of Selected Topics in Signal Processing. She is the recipient of the best paper award for 2016 INFOCOM Big Security WS and 2017 ICC. She received the B.S. degree in communication engineering from Nanjing University of Posts and Telecommunications, China, in 2000, the M.S.

degree in electrical engineering from Tsinghua University, China, in 2003, and the Ph.D. degree in electrical engineering from Rutgers University, NJ, in 2009. She was a visiting professor with Princeton University, Virginia Tech, and University of Maryland, College Park.



**Qingqing Wu** (S'13-M'16) received the B.Eng. and the Ph.D. degrees in Electronic Engineering from South China University of Technology and Shanghai Jiao Tong University (SJTU) in 2012 and 2016, respectively. He is currently an assistant professor in the Department of Electrical and Computer Engineering at the University of Macau, China, and also affiliated with the State key laboratory of Internet of Things for Smart City. He was a Research Fellow in the Department of Electrical and Computer Engineering at National University

of Singapore. His current research interest includes intelligent reflecting surface (IRS), unmanned aerial vehicle (UAV) communications, and MIMO transceiver design. He has published over 70 IEEE journal and conference papers. He was the recipient of the IEEE WCSP Best Paper Award in 2015, the Outstanding Ph.D. Thesis Funding in SJTU in 2016, the Outstanding Ph.D. Thesis Award of China Institute of Communications in 2017. He was the Exemplary Editor of IEEE Communications Letters in 2019 and the Exemplary Reviewer of several IEEE journals. He serves as an Associate Editor for IEEE Communications Letters, IEEE Open Journal of Communications Society, and IEEE Open Journal of Vehicular Technology. He is the Lead Guest Editor for IEEE Journal on Selected Areas in Communications on "UAV Communications in 5G and Beyond Networks", and the Guest Editor for IEEE Open Journal on Vehicular Technology on "6G Intelligent Communications" and IEEE Open Journal of Communications Society on "Reconfigurable Intelligent Surface-Based Communications for 6G Wireless Networks". He is the workshop co-chair for IEEE ICC 2019-2021 workshop on "Integrating UAVs into 5G and Beyond", and the workshop co-chair for IEEE GLOBECOM 2020 workshop on "Reconfigurable Intelligent Surfaces for Wireless Communication for Beyond 5G". He serves as the Workshops and Symposia Officer of Reconfigurable Intelligent Surfaces Emerging Technology Initiative and Research Blog Officer of Aerial Communications Emerging Technology Initiative.

This figure "Wu\_Qingqing.jpg" is available in "jpg" format from:

<http://arxiv.org/ps/2002.12271v4>

This figure "Xiao\_Liang.jpg" is available in "jpg" format from:

<http://arxiv.org/ps/2002.12271v4>

This figure "Zhao\_jun.jpg" is available in "jpg" format from:

<http://arxiv.org/ps/2002.12271v4>

# QoS-Driven Optimized Design in A New Integrated Visible Light Communication and Positioning System

Helin Yang<sup>1</sup>, Arokiaswami Alphones<sup>1</sup>, Wen-De Zhong<sup>1</sup>, Chen Chen<sup>2</sup>, Pengfei Du<sup>1</sup>, and Sheng Zhang<sup>1</sup>

<sup>1</sup>School of Electrical and Electronic Engineering, Nanyang Technological University, Singapore

<sup>2</sup>School of Microelectronics and Communication Engineering, Chongqing University, Chongqing, China

E-mail: {hyang013, ealphones, ewdzhong, and chen0884}@ntu.edu.sg

**Abstract**—This paper experimentally demonstrates a new integrated visible light communication and positioning (VLCP) system to support both the communication and positioning services. To maximize the system transmission data rate while meeting different quality-of-service (QoS) requirements of devices (minimum data rate and positioning accuracy constraints), a QoS-driven joint the adaptive modulation, subcarrier allocation and pre-equalization is presented to improve the system performance. The experimental results indicate that the presented integrated VLCP system achieve the higher positioning accuracy than the existing integrated VLCP system, and also verify that the proposed QoS-driven optimized design archives higher data rate, positioning accuracy and QoS satisfied probability, compared with other existing designs.

**Key Words**—Visible light communication and positioning, adaptive modulation, subcarrier allocation, weighted pre-equalization, quality-of-service (QoS).

## I. INTRODUCTION

WHITE light emitting diodes (LEDs) have attracted increasing attention in lighting markets, and it will gradually replace the conventional light elements for its long lifetime, energy efficiency and high security [1]. In addition, LEDs are widely applied for visible light communications (VLC) and visible light positioning (VLP) environments, such as office, supermarket, hospital and factory [1], [2].

On the one hand, LEDs enabled VLC is a promising technique for indoor communications with the merits of high data rate, no radio frequency (RF) interference and license-free operation. From now on, some techniques have been presented to overcome limited modulation bandwidth of VLC system and improve the system capacity, e.g., multiple-input multiple-output (MIMO) [3], [4], orthogonal frequency division multiplexing (OFDM) [5]-[9], as well as non-orthogonal multiple access (NOMA) [10]. In addition, considering that the signals modulated in the high-frequency subcarriers are seriously attenuated in VLC systems, adaptive transmission or frequency domain equalization techniques have been proposed to optimize the transmission parameters to enhance the system capacity [7]-[9], [11]-[15]. In [7]-[9], adaptive modulation designs combing with OFDM based on signal-to-noise-ratio (SNR) difference were studied in VLC systems to maximize the data rate, where lower-frequency subcarriers use high-order modulation levels with good SNR while the higher-frequency subcarriers apply lower-order modulation levels with poor SNR. To compensate the frequency attenuation, some pre-equalization schemes were proposed to establish high-speed VLC systems [11]-[15]. Li *et al.* experimentally demonstrated a hybrid time-frequency domain equalization design to overcome the nonlinearity and frequency attenuation of LEDs [11]. In [12] and [13], bit and power loading approaches were presented to combat the channel frequency selectivity. The

authors in [14] and [15] experimentally investigated weighted pre-equalization designs to enhance the system performance by compensating frequency attenuation of LEDs.

On the other hand, VLP based on LEDs has been applied for indoor positioning due to its low positioning error and economic compared with RF based indoor positioning systems [1], [2]. The literatures of [16]-[18] derived the positioning error by using received signal strength (RSS) positioning algorithm in VLP systems. The authors experimentally demonstrated differential phase difference of arrival (PDOA) [19] as well as low-complexity TDOA [20] based VLP systems, and experiments verified that the low positioning error can be achieved. Moreover, Zhang *et al.* experimentally evaluated a high positioning accuracy scheme based on angle of arrival (AOA) [21].

Recently, many works presented the integration of VLC and VLP in the same system [16], [22]-[24], called integrated VLCP system, in order to provide support both communication and positioning applications instead of supporting VLC [3]-[15] or VLP [2], [17]-[21] independently. In details, the references in [16] and [22] combined OFDM and RSS in integrated VLCP systems, but the performance might also be degraded due to severe out-of-band interference (OOBI) generated from OFDM signals. Additionally, an integrated VLCP system by applying filter bank multicarrier-based subcarrier multiplexing and PDOA was experimentally proposed in [23], which effectively reduced the OOBI and improved the system performance. Moreover, Yang *et al.* investigated the resource allocation for integrated VLCP systems with considering QoS constraints [24]-[26]. Unfortunately, quality-of-service (QoS) constraints (minimum data rate and positioning accuracy constraints) have not been experimentally studied in their works [3]-[26].

To solve the above mentioned challenges, this paper experimentally demonstrates a new integrated VLCP system model to improve the communication and positioning performance. After that, a QoS-driven optimized joint the adaptive modulation, subcarrier allocation and adaptive weighted pre-equalization is presented to optimize the system transmission data rate while ensuring different QoS requirements (minimum data rates and positioning accuracy requirements). Experimental results corroborate that the proposed integrated VLCP system and design achieve higher data rate, positioning accuracy and devices' QoS satisfaction levels, compared with other designs.

The rest of this paper is organized. A new integrated VLCP system is shown in Section II. Section III provides the principle of the proposed QoS-driven optimized design under devices' QoS requirements. The experimental results and discussion are shown in Section IV. Section V summarizes the

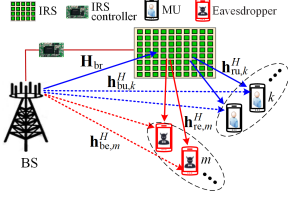


Fig. 1. The system models of integrated VLCP system.

article.

## II. INTEGRATED VLCP SYSTEMS MODEL

In indoor environments,  $L$  LED lamps, we call 'LED lamp' as 'LED' in some following descriptions) are attached on the ceiling to support the illumination requirements. In addition, they also set up an integrated VLCP system to support both communication and positioning services, and the corresponding signals are modulated on LED lamps and then pass through visible light channel. At each device, a photodetector (PD) is equipped to receive the optical signal before converting it into electrical signals.

In the integrated VLCP system system,  $K$  devices randomly distribute on the floor. The system has a central controller, which connects all LEDs to transmit signal to devices, and radio frequency (RF) is used to support uplink feedback. Once the central controller collects the feedback information, it can tackle the transmission scheduling task. We divide the total bandwidth into  $N$  subcarriers and  $L$  subcarriers are applied for positioning and other subcarriers are used for communication. The communication subcarriers is divided into  $K$  groups (subcarrier group, called SG) and the  $(K+1)$ -th SG being the subcarriers used for RSS positioning. In addition, a transmission diversity method is applied, where all LEDs transmit same communication signal if one communication subcarrier is allocated to a device.

This section mainly describe one existing popular VLCP system and describes a new integrated VLCP system. In addition, both the communication and positioning models are provided in detail.

### A. Proposed Integrated VLCP System Model

1) *OFDMA based VLCP with RSS [16]*: The design combines the OFDM technique and two dimensional (2D) RSS positioning to establish integrated VLCP systems, as illustrated in Fig. 1 (a), where the total available subcarriers are equally divided into four subbands and allocate them to four LED lamps. Then, its corresponding LED lamp has one subband and it also is employed to perform positioning. The more details to realize OFDMA based VLCP with RSS can be found in [16]. However, from Fig. 1 (a), we find that OFDM signals leakage relatively severe OOB to adjacent subbands or subcarriers, which may degrade the system performance in integrated VLCP systems. In addition, we can observe that the bandwidth utilization efficiency of this system is not effective, because each LED lamp only uses a part of the bandwidth.

2) *Presented OFDM-SCM-interleaving based VLCP with RSS*: From Fig. 1 (b) [26], we find that when the  $L$  subcarriers

are not used for communication signal transmitting (idle subcarriers), there has  $L$  specific frequency holes which have negligible OOB from OFDM signal. Hence, RSS positioning signals (blue color) can be modulated on the frequency holes, which has the ability to avoid OOB on positioning frequencies from adjacent communication subcarriers and decrease the effect of OOB on the positioning accuracy compared with OFDMA based VLCP. In addition, it has the higher effective bandwidth utilization than that of OFDMA based VLCP. It is noting that our previous work [26] did not apply transmission diversity to enhance the desired received signal, while this model adopts transmission diversity with lower complexity compared with the work [26].

### B. Communication Model

In integrated VLCP system, the line-of-sight (LOS) optical channel gain from the  $l$ -th LED lamp to the  $k$ -th device is expressed as

$$G_{k,l} = \frac{(m_l + 1)A_r}{2\pi d_{k,l}^2} \cos^{m_l}(\phi_{k,l}) T_s(\psi_{k,l}) g(\psi_{k,l}) \cos\psi_{k,l} \quad (1)$$

where  $A_r$  is the PD' active area.  $d_{k,l}$ ,  $\phi$  and  $\psi_{k,l}$  are the distance, the angle of irradiance and the angle of incidence between LED lamp LED  $l$  and device  $k$ , respectively.  $m_l$  represents the order of Lambertian emission of the  $l$ -th LED lamp, which can be measured in the experimental preparation [18].  $T_s(\psi_{k,l})$  and  $g(\psi_{k,l})$  denote the gain of the optical filter and the concentrator gain at PD, respectively.

At the receiver, the received SNR of maximum ratio combining (MRC) for the  $k$ -th device on communication subcarrier  $n$  is expressed as

$$\gamma_{k,n}^{\text{co}} = \mu^2 \sum_{n=l}^L P_{n,l} (G_{k,n,l})^2 / \delta^2 \quad (2)$$

where  $\mu$  denotes the PD's responsivity.  $P_{n,l}$  is the allocated electrical power on subcarrier  $n$  at LED lamp  $l$ .  $G_{k,n,l}$  is the channel gain from LED lamp  $l$  to device  $k$  on subcarrier  $n$ .  $\delta^2$  denotes the additive background noise power containing the shot noise and the thermal noise [6].

At the  $k$ -th device (receiver), if it is assigned the  $n$ -th subcarrier and the OFDM signal is modulated by  $M_n$ -quadrature amplitude modulation (QAM) with the modulation order  $M_n$ , the bit error rate (BER) is defined by adopting [6],

$$BER_{k,n} = \frac{\sqrt{M_n} - 1}{\sqrt{M_n} \log_2(\sqrt{M_n})} \text{erfc} \left( \sqrt{\frac{3\gamma_{k,n}^{\text{co}}}{2(M_n - 1)}} \right) \quad (3)$$

The sum transmission data rate (bps) of all devices across all the subcarriers can be given by [6]

$$R_{\text{sum}} = B_{\text{sub}} \sum_{n=1}^{N/2-1} \log_2 M_n \quad (4)$$

where  $B_{\text{sub}}$  denotes subcarrier bandwidth  $B_{\text{sub}} = B/N$ , where  $B$  denotes the transmission bandwidth. In (4), in the system, the IFFT/FFT size is  $N$ , and the number of available subcarriers is  $N/2-1$  due to the Hermitian symmetry [6], [7].

### C. Positioning Model based on RSS

At device  $k$ , the received power on positioning subcarrier  $i$  from lamp  $l$  can be written as  $P_{k,i,l}^{\text{rec}} = G_{k,l} P_{i,l}$  [16]-[18]. Since the PD axis and the LED lamp axis are perpendicular to the ceiling, we can get  $\cos(\phi_{k,l}) = \cos\psi_{k,l} = h/d_{k,l}$ , where  $h$  denotes the height from LED lamps to the devices [16]-[18]. Hence,  $G_{k,l}$  in (1) is rewritten as

$$G_{k,l} = \frac{h^{m_l+1}(m_l+1)A_r}{2\pi d_{k,l}^{m_l+3}} T_s(\psi_{k,l})g(\psi_{k,l}) = C(m_l+1) \frac{h^{m_l+1}}{d_{k,l}^{m_l+3}} \quad (5)$$

where  $C = A_r T_s(\psi_{k,l})g(\psi_{k,l})/2\pi$  is a constant parameter and it is determined by the characteristics of VLCP systems. Based on (5),  $P_{k,i,l}^{\text{rec}}$  is derived as

$$P_{k,i,l}^{\text{rec}} = P_{i,l} C(m_l+1) h^{m_l+1} / d_{k,l}^{m_l+3} \quad (6)$$

From (6), we derive the distance  $d_{k,l}$  as

$$d_{k,l} = \sqrt[m_l+3]{P_{i,l} C(m_l+1) h^{m_l+1} / P_{k,i,l}^{\text{rec}}} \quad (7)$$

In fact, in practical indoor systems, it is quite hard to find the accurate relationship between estimated distance and the received positioning power like Eq(7). Therefore, the final estimated distance can be polyfit by a function, such as the formulated polyfit function shown in Eq. (10) in [22]. Hence, the final estimated distance  $d_{k,l}$  can be expressed as a function with respect to the received positioning power  $P_{k,i,l}^{\text{rec}}$ , which is

$$d_{k,l} = Q_l(P_{k,i,l}^{\text{rec}}) \quad (8)$$

We would like to mention that each LED lamp has its corresponding function  $Q_l(\cdot)$ , because the order of Lambertian emission ( $m_l$ ) of each LED lamp and the attenuation of its corresponding positioning frequency is different from each other [18], [22]. As mentioned, it is difficult to find the accurate relationship between the estimated distance and the measured received positioning power (i.e, Eq. (8)). Hence, we take measurements at a number of points during the offline preparation in the integrated VLCP system to obtain Eq. (8) before estimating the positions of devices, more details can be found in [22].

Once  $P_{k,i,l}^{\text{rec}}$  is measured at the  $k$ -th device, the distance  $d_{k,l}$  is obtained by using (8). After calculating  $d_{k,l}$ , the estimated location of each device can be computed by adopting the RSS-based positioning algorithm [16]-[18], the more procedures to experimentally realize RSS-based positioning can be found in [18], [22]. Let  $\Theta_k = (x_k, y_k)$  and  $\Theta_k^e = (x_k^e, y_k^e)$  denote the true location and the estimated location of device  $k$ , respectively. The positioning error of device  $k$  can be expressed as

$$PE_k = \sqrt{(x_k^e - x_k)^2 + (y_k^e - y_k)^2} \quad (9)$$

## III. QoS-DRIVEN OPTIMIZED DESIGN FOR INTEGRATED VLCP SYSTEMS

### A. QoS Requirements of Indoor Devices

In integrated VLCP systems, piratical QoS requirements of devices need to be taken into account, which are discussed in this subsection:

1) *Minimum data rate requirements*: Some indoor devices have the minimum data rate requirement, where this requirement needs to be ensured in integrated VLCP systems. Hence, the resulting requirement is given by

$$R_k = B_{\text{sub}} \sum_{n=1}^{N/2-1} (\rho_{k,n} \log_2 M_n) \geq R_k^{\text{min}} \quad (10)$$

where  $R_k$  and  $R_k^{\text{min}}$  are the current achievable data rate and the minimum data rate threshold of the  $k$ -th device, respectively;  $\rho_{k,n}$  denotes a binary variable,  $\rho_{k,n} \in \{0, 1\}$ , and  $\rho_{k,n} = 1$  indicates communication subcarrier  $n$  is allocated to the  $k$ -device; otherwise, it  $\rho_{k,n} = 0$ .

2) *Positioning accuracy requirements*: In addition to the requirement in (10) of VLC, integrated VLCP systems need to satisfy the positioning accuracy constraint of the devices who apply positioning services.

Generally, when other parameters of the integrated VLCP system are fixed, the positioning error (PE) can be written as an explicit function of transmit power vector by adopting Cramer-Rao Lower Bound (CRLB) [27]. Accordingly, the CRLB on PE of device  $k$  is expressed as [27]

$$PE_k^{\text{CRLB}} \geq \sqrt{\text{tr}(\mathbf{J}^{-1}(\Theta_k^e, \mathbf{P}_{\text{po}}))} \quad (11)$$

where  $\mathbf{J}(\cdot)$  denotes fisher information matrix and  $\mathbf{P}_{\text{po}}$  represents the transmit power vector on positioning subcarriers at four LED lamps. More details of the derivation and proof, please see [26] and [27] for the comprehensive analysis. Finally, we can get the following constraint

$$\sqrt{\text{tr}(\mathbf{J}^{-1}(\Theta_k^e, \mathbf{P}_{\text{po}}))} \leq PE_k^{\text{max}} \quad (12)$$

where  $PE_k^{\text{max}}$  denotes the maximum positioning error threshold of device  $k$ .

### B. QoS-Driven Adaptive Transmission Design

The block diagram of the proposed QoS-driven optimized design for integrated VLCP systems is illustrated in Fig. 2 (we take the system mode shown in Fig. 1(b) as an example), where the joint adaptive modulation, subcarrier allocation and adaptive weighted pre-equalization is presented to guarantee the QoS constraints expressed in (10) and (12). The process to realize the adaptive transmission are provided by the following analysis.

At the transmitters, the system allocates communication SGs to devices, and then the sinusoidal signals for VLP are added with OFDM signal at each LED lamp, where four positioning frequencies from  $f_1$  to  $f_4$  are set into the  $(K+1)$ -th SG and all communication signals are allocated on  $K$  SGs. The central controller receives the information (e.g., channel state information, channel quality, and QoS requirements) from devices, and it selects the adaptive  $M$ -QAM mapping according to devices' different minimum data requirements

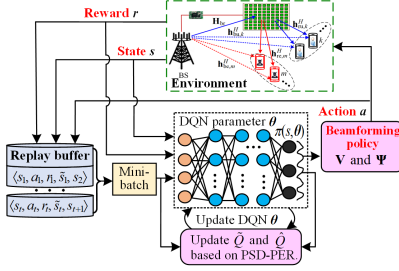


Fig. 2. Block diagram of the proposed QoS-driven optimized design for integrated VLCP systems.

and feedback information. Let  $BER_{max}$  denote the  $BER$  target, the modulation threshold is defined as [6], [7]

$$\begin{aligned} \gamma_j^{\text{th}} &= (\gamma_{k,n}^{\text{co}})_{M_n} \\ &= \frac{3(M_n-1)}{2} \text{erfc}^{-1} \left( BER_{\text{max}} \frac{\sqrt{M_n} \log_2(\sqrt{M_n})}{\sqrt{M_n-1}} \right) \\ M_n &= 2^j, j = 1, \dots, J \end{aligned} \quad (13)$$

where  $\text{erfc}^{-1}(\cdot)$  denotes the inverse  $\text{erfc}$ -function, and  $\gamma_1^{\text{th}} \leq \gamma_2^{\text{th}} \leq \dots \leq \gamma_J^{\text{th}}$ . According to (13), the system chooses the modulation order based on SNR value  $\gamma_{k,n}^{\text{co}}$ , which is

$$M_n = \begin{cases} 0, & \gamma_{k,n}^{\text{co}} < \gamma_1^{\text{th}} \\ 2^j, & \gamma_j^{\text{th}} \leq \gamma_{k,n}^{\text{co}} \leq \gamma_{j+1}^{\text{th}}, j = 1, \dots, J-1 \\ 2^J, & \gamma_J^{\text{th}} \leq \gamma_{k,n}^{\text{co}}. \end{cases} \quad (14)$$

The above analysis from (13) and (14) just shows the modulation order selection process based on the received SNR information from devices.

Considering the fact that the severe attenuation of LED lamps in high frequency domain in integrated VLCP systems, the pre-equalization design is adopted to compensate the frequency attenuation at transmitters. We find that transitional pre-equalization methods are not optimal, because the system sacrifices a large amount of power to balance of the attenuation in high frequency domains. The authors in [15] proposed a weighted pre-equalization scheme to optimize the sum data rate of all subbands. However, weighted pre-equalization in [15] was still not the optimal scheme, because it is a only fixed-order modulation format and fixed bandwidth of each sub-band. Moreover, the weighted pre-equalization factor for the positioning SG needs to be carefully design to guarantee the positioning accuracy constraints, because transmission power allocated on the two adjacent communication SGs near the positioning SG should not be too large to generate severe OOB on the positioning SG, which will degrade the positioning accuracy. Therefore, the joint adaptive modulation, subcarrier allocation as well as weighted pre-equalization are dynamically optimized to improve the system data rate while ensuring different QoS requirements.

Let  $M_k$  denotes the modulation order in SG  $k$ . Let  $\rho_k$  denotes the subcarrier allocation indicator vector for  $k$ -th device in the  $k$ -th SG and we set that these subcarriers are continuous. Then, the  $k$ -th SG signal in the frequency domain after implementing the joint adaptive modulation, subcarrier allocation, as well as weighted pre-equalization can

be expressed by

$$\mathbf{S}'_k(M_k, \rho_k) = W_k \cdot \mathbf{H}_k^{-1}(\rho_k) \cdot \mathbf{S}_k(M_k, \rho_k) \quad (15)$$

where  $\mathbf{S}'_k(M_k, \rho_k)$  and  $\mathbf{S}_k(M_k, \rho_k)$  are the  $k$ -th SG signal vector before and after pre-equalization, respectively.  $W_k$  and  $\mathbf{H}_k$  are the weighted pre-equalization coefficient and the transfer function matrix of the  $k$ -th SG, respectively. It is worth noting that  $\mathbf{H}_k$  is a diagonal matrix.  $\mathbf{H}_k$  can be measured offline before the experiment. Then, the pre-equalized signals are transformed into the time domain before being modulated on the LED lamps.

At each device, for VLP, the received power values on the four positioning frequencies from four corresponding LED lamps can be measured in OFDM-SCM-interleaving based VLCP. After measuring the four received positioning power values, the position of the device is calculated by adopting the RSS-based positioning method, which has been analyzed in Section III.C. For VLC, the communication signals are achieved when the received signals are filtered by using band stop filter (BSF), and finally communication signals are demodulated by adopting OFDM demodulation technique.

In practical indoor environments, different devices have different QoS requirements, such as low positioning error constraints and the high transmission data rate requirements. The system aims to optimize the transmission data rate while satisfying different QoS requirements expressed in (10) and (12), the detailed procedures to implement it are shown as follows:

**Step 1:** The central controller collects the feedback information from devices, which mainly refers to channel information, SNR values, QoS requirements, etc.;

**Step 2:** The central controller iteratively optimize the subcarrier allocation indicators  $\{\rho_k\}$ , the weighted pre-equalization coefficients  $\{W_k\}$  and the modulation orders  $\{M_k\}$  to the satisfy the minimum data rate requirements in (10) and the positioning accuracy constraints in (12) first, by using the iteration algorithm [12], [13];

**Step 3:** After satisfying the QoS requirements of devices, the extra power and subcarriers are allocated to the devices with highest channel quality to optimize the transmission data rate by updating  $\{\rho_k\}$ ,  $\{W_k\}$  and  $\{M_k\}$ .

#### IV. EXPERIMENTAL SETUP AND RESULTS

As shown in Fig. 3, the experimental setup is provided to evaluate the system performance. We use MATLAB to

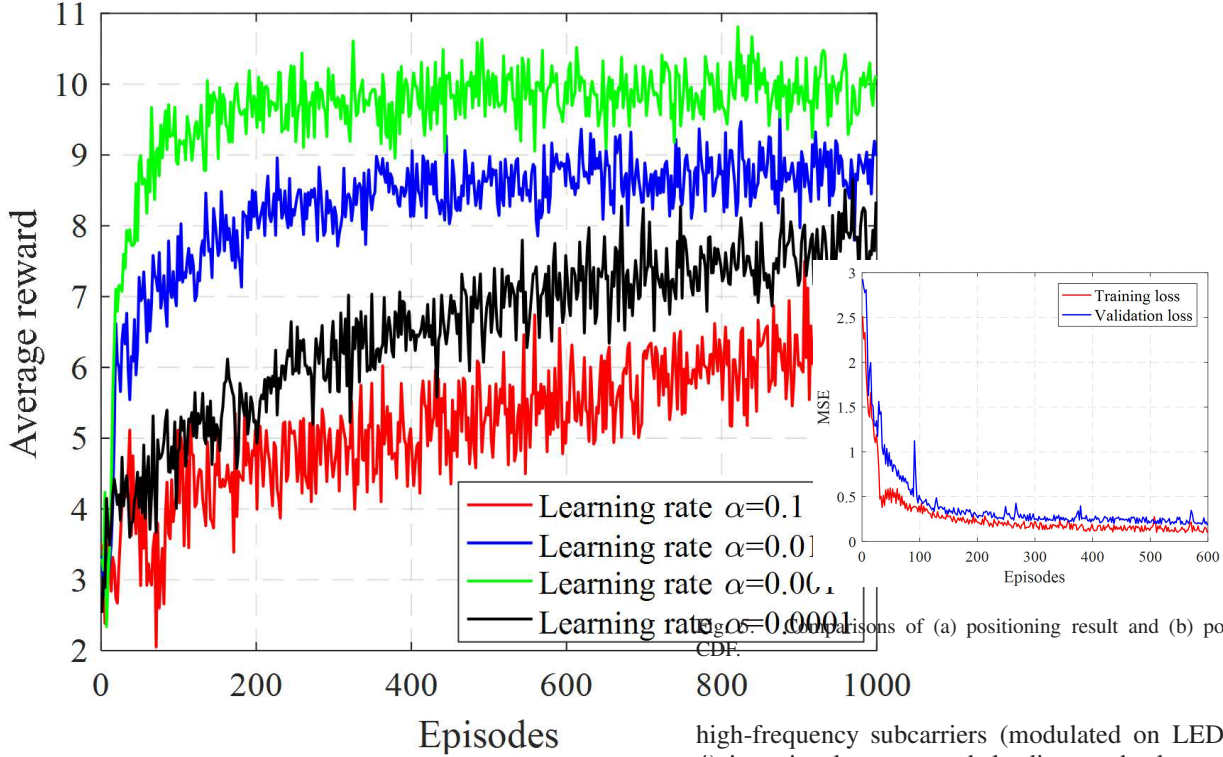


Fig. 4. Received spectra of (a) proposed integrated VLCP and (b) existing integrated VLCP [16].

generated the integrated communication and positioning signal with an IFFT size of 512, then load the signal in an arbitrary waveform generator, before adding it to the DC bias of the four LED lamps (LXK8-PW27-0016) after passing through the amplifiers and adding DC biases. After passing through optical wireless channel, the light is detected by using an avalanche PD before using a digital storage oscilloscope to record the detected signal. After that, the communication signal demodulation and the device location estimation are completed by using MATLAB. The experiment is in a coverage area of  $2 \times 2 \times 1.35 \text{ m}^3$ . The locations of four LED lamps are  $(-0.4, 0.4, 1.35)$ ,  $(0.4, 0.4, 1.35)$ ,  $(-0.4, 0.4, 1.35)$  and  $(-0.4, -0.4, 1.35)$  with the origin  $(0, 0, 0)$  in meters. The modulation bandwidth we use is 20 MHz. The four positioning frequencies are at 5.19, 5.31, 5.43, and 5.55 MHz, respectively. The modulation order  $M = \{2, 4, 8, 16, 32\}$  and  $BER_{\max} = 3.8 \times 10^{-3}$ . Four devices locate on the receiving plane, two of them require both communication and positioning services and each has the data rate requirement (1 Mbit/s), while other two devices only need communication services and each has the high data rate requirement (12.5 Mbit/s). Then, the total data rate requirement is 27 Mbit/s. The tolerant positioning error threshold is 10 cm.

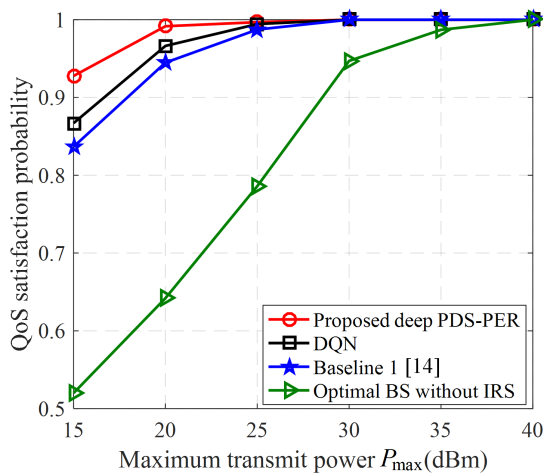
Fig. 4 (a) and (b) indicate the received spectrum of the integrated signals in FBMC-SCM-interleaving and OFDMA based integrated VLCP systems when the device locates at  $(0\text{m}, 0\text{m}, 0\text{m})$ , respectively. In Fig. 4 (b), the power in the

high-frequency subcarriers (modulated on LED 3 and LED 4) is seriously attenuated, leading to the low received SNR, which degrades the positioning accuracy in the existing design [16]. By contrast, our proposed design has high SNR values for all positioning subcarriers to guarantee the positioning performance. In addition, OFDMA based VLCP in [16] has high OOBIs to adjacent subbands and it needs guard bands (G-Bs), while our design has negligible OOBIs on the positioning frequency holes.

Fig. 5 (a) and (b) show the positioning errors distributions over the area and the corresponding Cumulative Distribution Function (CDF), respectively. In Fig. 5 (a), we find that positioning error is low at the center areas, but is high at the edges or corners, because of the decreased received power. The mean position errors of our proposed design and the existing design [16] are 6.88 cm and 10.56 cm, respectively, which indicates the higher positioning accuracy achieved by our proposed design. In Fig. 5 (b), when  $RSE^{\max} = 10$  cm, our design has the probability of 84.26 % to meet devices' positioning accuracy constraints, while the design in [16] only has the probability of 42.43 %.

Fig. 6 illustrates the data rate and QoS satisfaction level versus the bias input current for the three designs (Note: W-p-eq. means weighted pre-equalization and AM denotes adaptive modulation). As the increase of the input current, the sum data rate performance increases due to the high received SNR. Our proposed design (OFDM-SCM-interleaving w/ Joint) outperforms the design in [15] (OFDM-SCM-interleaving w/ Wei-pre-eq.AM), because we consider subcarrier allocation in the transmission optimization design. However, the data rate performance of the design in [16] is worse, the main reasons are listed as follows: 1) it has low effective bandwidth utilization when the total bandwidth is equally divided into

(a)



(b)

Fig. 6. Sum data rate vs. bias current (mA).

four subbands for four LED lamps as shown in Fig 2 (a) and the analysis shown in Section II.A; 2) Four LED lamps transmit their signals independently in four subbands, which exists high OOB at the edge of each sub-band, so it needs some number of subcarriers as GBs. Hence the low effective bandwidth utilization degrades the data rate performance in the design [16]. From Fig. 6(b), we can observe that our proposed design can effectively satisfy the QoS requirements.

## V. CONCLUSION

This paper presented and experimentally verify an integrated VLCP system model to enhance both communication and positioning performance. A QoS-driven optimized joint the adaptive modulation, subcarrier allocation and adaptive weighted pre-equalization was presented to ensure the different QoS requirements. The experimental results illustrated that the presented integrated VLCP system model improves the data rate and positioning accuracy compared with existing adaptive transmission designs. In the future, we will pay more attention to how to extend the proposed system model in multi-cell scenario and consider piratical LoS links blockages into account.

## VI. ACKNOWLEDGEMENTS

This work is support by Delta-NTU Corporate Lab for Cyber-Physical Systems with funding support from Delta Electronics Inc. and the National Research Foundation (NRF) Singapore under the Corp Lab@University Scheme, and National Natural Science Foundation of China under Grant 61901065.

## REFERENCES

- [1] A. Jovicic, L. Junyi, and T. Richardson, "Visible light communication: opportunities, challenges and the path to market," *IEEE Commun. Mag.*, vol. 51, no. 12, pp. 26-32, Dec. 2013.
- [2] M. F. Keskin, A. D. Sezer, and S. Gezici, "Localization via visible light systems," *Proc. IEEE*, vol. 106, no. 6, pp. 1063-1088, Jun. 2018.
- [3] L. Zeng, *et al.*, "High data rate multiple input multiple output (MIMO) optical wireless communications using white led lighting," *IEEE J. Sel. Areas Commun.*, vol. 27, no. 9, pp. 1654-1662, Dec. 2009.
- [4] H. Yang, C. Chen, W.-D. Zhong, and A. Alphones, "Joint precoder and equalizer design for multi-user multi-cell MIMO VLC systems," *IEEE Trans. Veh. Technol.*, vol. 67, no. 12, pp. 11354-11364, Dec. 2018.

- [5] D. Tsonev, *et al.*, "A 3-Gb/s single-LED OFDM-based wireless VLC link using a gallium nitride LED," *IEEE Photon. Technol. Lett.*, vol. 26, no. 7, pp. 637-640, Apr. 2014.
- [6] R. Mesleh, H. Elgala, and H. Haas, "On the performance of different OFDM based optical wireless communication systems," *IEEE/OSA J. Opt. Commun. Netw.*, vol. 3, no. 8, pp. 620-628, Aug. 2011.
- [7] L. Wu, Z. Zhang, J. Dang, and H. Liu, "Adaptive modulation schemes for visible light communications," *J. Lightw. Technol.*, vol. 33, no. 1, pp. 117-125, 1 Jan. 2015.
- [8] J. He, J. He, and J. Shi, "An enhanced adaptive scheme with pairwise coding for OFDM-VLC system," *IEEE Photon. Technol. Lett.*, vol. 30, no. 13, pp. 1254-1257, Jul. 2018.
- [9] X. Huang, *et al.*, "2.0-Gb/s Visible light link based on adaptive bit allocation OFDM of a single phosphorescent white LED," *IEEE Photon. J.*, vol. 7, no. 5, pp. 1-8, Oct. 2015.
- [10] C. Chen, W. Zhong, H. Yang, P. Du, and Y. Yang, "Flexible-rate SIC-free NOMA for downlink VLC based on constellation partitioning coding," *IEEE Wireless Commun. Lett.*, vol. 8, no. 2, pp. 568-571, Apr. 2019.
- [11] Z. Li and C. Zhang, "An improved FD-DFE structure for downlink VLC systems based on SC-FDMA," *IEEE Commun. Lett.*, vol. 22, no. 4, pp. 736-739, Apr. 2018.
- [12] G. Zhang, Ju. Zhang, X. Hong, and S. He, "Low-complexity frequency domain nonlinear compensation for OFDM based high-speed visible light communication systems with light emitting diodes," *Opt. Express*, vol. 25, no. 4, pp. 3780-3794, Feb. 2017.
- [13] H. Chen, Z. Xu, Q. Gao and S. Li, "A 51.6 Mb/s experimental VLC system using a monochromic organic LED," *IEEE Photon. J.*, vol. 10, no. 2, pp. 1-12, Apr. 2018.
- [14] Y. Hong, J. Xu, and L. Chen, "Experimental investigation of multi-band OCT precoding for OFDM-based visible light communications," *Opt. Express*, vol. 25, no. 17, pp. 12908-12914, May 2017.
- [15] Y. Wang, L. Tao, Y. Wang, and N. Chi, "High speed WDM VLC system based on multi-band CAP64 with weighted pre-equalization and modified CMMA based post-equalization," *IEEE Commun. Lett.*, vol. 18, no. 10, pp. 1719-1722, Oct. 2014.
- [16] Y. Xu, Z. Wang, P. Liu, J. Chen, S. Han, C. Yu, and J. Yu, "Accuracy analysis and improvement of visible light positioning based on VLC system using orthogonal frequency division multiple access," *Opt. Express*, vol. 26, no. 7, pp. 9230-9242, Apr. 2018.
- [17] W. Gu, M. Aminikashani, P. Deng, and M. Kavehrad, "Impact of multipath reflections on the performance of indoor visible light positioning systems," *J. Lightw. Technol.*, vol. 34, no. 10, pp. 2578-2587, May 2016.
- [18] F. Alam, M. T. Chew, T. Wenge, *et al.*, "An accurate visible light positioning system using regenerated fingerprint database based on calibrated propagation model," appear in *IEEE T. Instrum. Meas.*.
- [19] S. Zhang, W.-D. Zhong, P. F. Du, and C. Chen, "Experimental demonstration of indoor sub-decimeter accuracy VLP system using differential PDOA," *IEEE Photon. Technol. Lett.*, vol. 30, no. 19, pp. 1703-1706, Oct. 2018.
- [20] P. Du, S. Zhang, C. Chen, and W. Zhong, "Demonstration of a low-complexity indoor visible light positioning system using an enhanced TDOA," *IEEE Photon. J.*, vol. 10, no. 4, pp. 1-10, Aug. 2018.
- [21] R. Zhang, W. Zhong, K. Qian, and D. Wu, "Image sensor based visible light positioning system with improved positioning algorithm," *IEEE Access*, vol. 5, pp. 6087-6094, Feb. 2017.
- [22] B. Lin, X. Tang, Z. Ghassemlooy, C. Lin, and Y. Li, "Experimental demonstration of an indoor VLC positioning system based on OFDMA," *IEEE Photon. J.*, vol. 9, no. 2, pp.1-9, Apr. 2017.
- [23] H. Yang, C. Chen, W.-D. Zhong, A. Alphones, S. Zhang, and P. Du, "Demonstration of a quasi-gapless integrated visible light communication and positioning system," *IEEE Photon. Technol. Lett.*, vol. 30, no. 23, pp. 2001-2004, Dec. 2018.
- [24] H. Yang, *et al.*, "Resource allocation for multi-user integrated visible light communication and positioning systems," in *Proc. IEEE Int. Conf. Commun. (ICC)*, Shanghai, China, 2019, pp. 1-6.
- [25] H. Yang, *et al.*, "Reinforcement learning based intelligent resource allocation for integrated visible light communication and positioning systems," Appear in *IEEE Wireless Commun. Lett.*, vol. 8, no. 4, pp. 1204-1207, Aug. 2019.
- [26] H. Yang, W. Zhong, C. Chen, A. Alphones, and P. Du, "QoS-driven optimized design-based integrated visible light communication and positioning for indoor IoT networks," *IEEE Internet Things J.*, vol. 7, no. 1, pp. 269-283, Jan. 2020.
- [27] M. F. Keskin and S. Gezici, "Comparative theoretical analysis of distance estimation in visible light positioning systems," *J. Lightw. Technol.*, vol. 34, no. 3, pp. 854-865, Feb. 2016.